Macrophage-mediated resistance mechanisms against MAPK inhibitory cancer therapeutics

by

Stephanie Joy Wang

B.S., University of California, Los Angeles (2014)

Submitted to the Department of Biological Engineering
in partial fulfillment of the requirements for the degree of

Doctor of Philosophy

at the

MASSACHUSETTS INSTITUTE OF TECHNOLOGY

June 2019

Signature redacted

Author .....
Department of Biological Engineering
May 10, 2019

Signature redacted

Certified by .....
Douglas A. Lauffenburger
Ford Professor of Biological Engineering, Chemical Engineering, and Biology
Head, Department of Biological Engineering
Thesis Supervisor

Signature redacted

Accepted by .....
Forest M. White
Professor of Biological Engineering
Chairman, Graduate Program Committee

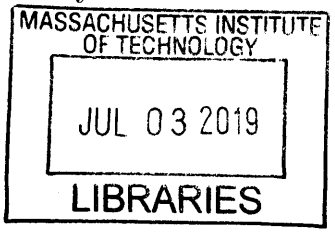

ARCHIVES

This doctoral thesis has been examined by a Committee of the Department of Biological Engineering as follows:

Douglas A. Lauffenburger
Thesis Supervisor
Ford Professor of Biological Engineering
Massachusetts Institute of Technology

Forest M. White
Chairman, Thesis Committee
Professor of Biological Engineering
Massachusetts Institute of Technology

K. Dane Wittrup
Member, Thesis Committee
Professor of Biological Engineering
Massachusetts Institute of Technology

Ryan J. Sullivan
Member, Thesis Committee
Assistant Professor of Medicine
Harvard Medical School

Macrophage-mediated resistance mechanisms against MAPK inhibitory cancer therapeutics

by

Stephanie Joy Wang

Submitted to the Department of Biological Engineering
on May 10, 2019, in partial fulfillment of the
requirements for the degree of
Doctor of Philosophy

Abstract

Kinase inhibitors targeting the MAPK pathway are often limited by lack of durable clinical responses or, in many cancer types, lack of even initial responses. While great headway has been made on characterizing mechanisms of resistance, understanding the full influence of complex intercellular interactions on drug resistance remains a challenge. Here, we combine computation with experiment to investigate the cellular and molecular contributions of the tumor microenvironment to MAPK inhibitor response.

First, we employ a computational framework using published bulk and single-cell patient gene expression data to investigate immune cell correlates of MAPK inhibitor resistance, and subsequently quantify potential intercellular ligand-receptor interactions between cell populations of interest. Next, we use multiplex proteomic immunoassays and co-culture experiments to characterize the impact of these interactions on tumor-intrinsic bypass signaling and phenotype. To assess the in vivo relevance of these multicellular and multidirectional signaling networks, we develop an intravital imaging strategy to monitor the influence of tumor-associated macrophages on cancer cell kinase activity dynamics. Finally, we rationally design a nanotherapy to exploit inhibitor-induced immunomodulation and crosstalk.

Overall, we present a paradigm to systematically dissect signaling pathways between tumors and their microenvironments, validate these interactions in various models of disease, and design therapeutic strategies to target them.

Thesis Supervisor: Douglas A. Lauffenburger
Title: Ford Professor of Biological Engineering, Chemical Engineering, and Biology

Acknowledgments

This work would not have been possible (and my Ph.D. journey would not have been nearly as enjoyable) without the help and support of many people.

First and foremost, I would like to thank my thesis advisor, Douglas Lauffenburger. Doug has not only provided me with the freedom and resources to pursue my research, but also actively supported my career development throughout the years. He somehow always found a way to make time for his students and continually provided thoughtful guidance along the way.

I would also like to extend my gratitude to other mentors I have had while at MIT. Miles Miller (Massachusetts General Hospital) has acted as an unofficial advisor, and my thesis committee members, Forest White, Dane Wittrup, and Ryan Sullivan (Harvard Medical School) have provided a variety of perspectives leading to more impactful project directions. I thank Daniel Kamei (University of California, Los Angeles) for piquing my interest in cancer signaling through an all-encompassing undergraduate research experience, and Daniel Kirouac (formerly Genentech, Inc.) for mentoring me during a summer internship, where I applied quantitative systems pharmacology towards drug development efforts.

I am grateful to my colleagues at MIT for their immense scientific and personal support. I thank Allison Claas, Annelien Zweemer, Sarah Schrier, Abby Hill, Jorge Valdez, Simon Gordonov, Madeleine Oudin, and Aaron Meyer for helping me become acquainted with graduate-level research and providing feedback on the early stages of my thesis project. Brian Joughin, Evan Chiswick, Simona Dalin, Alina Starchenko, Manu Kumar, and Doug Brubaker have been more than helpful with continued input at our weekly data meetings. Alex Brown, Charlotte Fonta, and Alex Wang have provided stimulating discussions and made times in lab all the merrier, while Linda Stockdale and Julia Papps contributed to a great work environment. Additionally, over all these years, Hsinhwa Lee has made sure that I never had to worry about anything in lab other than my research.

I spent most of my time during the last year of graduate school at the Massachusetts General Hospital Center for Systems Biology. I thank my colleagues there, including but not limited to Mark Prytyskach, Ran Li, Thomas Ng, Gaurav Luthria, Rainer Kohler, and Stefan Kronister, for providing me with significant technical assistance across a broad range of scientific disciplines.

Finally, I thank my family and friends, both near and far, for being unwavering sources of support and encouragement.

Contents

List of Figures

1 Introduction

1.1 Receptor tyrosine kinase (RTK) signaling in cancer

1.1.1 RTK hyperactivity

Many of the 58 known human RTKs serve as key regulators of critical cellular processes including cell-cycle control, metabolism, survival, proliferation, and migration. All members of this cell-surface receptor family have a similar molecular structure, with extracellular N-terminal ligand-binding domains, a single transmembrane helix, and a cytoplasmic tyrosine kinase domain. [1] Binding of RTKs to their cognate ligands stabilizes the conformation of receptor molecules as active dimers or oligomers, enabling phosphorylation of tyrosine(s) within the kinase domain of its RTK neighbor(s), as well as the release of cis-autoinhibition. The phosphorylated tyrosine kinase domains then serve as docking sites for recruitment, assembly, and activation of downstream signaling mediators. [2]

Under normal physiological conditions, RTK activity is tightly regulated by mechanisms such as dephosphorylation via protein tyrosine phosphatases, inhibitory serine phosphorylation, and/or degradation following endocytosis. [3–5] For many RTKs, activation normally accelerates the rates of RTK internalization as well as sorting to late endosomes and lysosomes for proteolytic degradation,

while possibly reducing the rate of recycling back to the cell surface.

The aforementioned check and balances associated with normal receptor signaling can be overcome by a few primary mechanisms of RTK hyperactivity in cancer: gain-of-function mutations, overexpression, or chromosomal rearrangements. [6] Gain-of-function mutations typically cluster in evolutionarily conserved residues with key roles in ATP binding and catalytic activity, but can also occur in other RTK domains. Some of the most well-known examples include the small in-frame deletions within exon 19 or L858R point mutation for EGFR. [7] Overexpression arises primarily via gene amplification, which increases the copy number of a specific genomic region, but can also be due to upregulation of transcriptional or translational processes, as well as loss of microRNA-mediated gene silencing. RTK overexpression has been described in many cancers, including ERBB2 in breast and ovarian cancers, MET in lung cancer, and AXL in glioblastoma. [8–11] Additionally, chromosomal rearrangements leading to the formation of novel tyrosine kinase fusion oncoproteins have been identified. The first-discovered and most often-cited example is the t(9,22) translocation, which fuses the ABL1 tyrosine kinase gene on chromosome 9 to the BCR gene on chromosome 22 to form the BCR-ABL fusion, primarily found in chronic myeloid leukemia. [12]

1.1.2 Growth factor-induced RTK activation

Growth factors are compact polypeptides that bind to cell-surface RTKs in order to stimulate cellular responses. Non-transformed cells have an absolute requirement for growth factors to proliferate, while transformed cells may possess activating RTK genetic alterations that can elicit ligand-independent signaling. [13] However, especially in cases where the relevant oncogenic RTKs are only overexpressed and not mutated, cancer cells can still depend on growth factors for growth and metastatic dissemination. Growth factors may be secreted via exocytosis pathways or, as is the case with the EGFR ligand family, they may be synthesized as

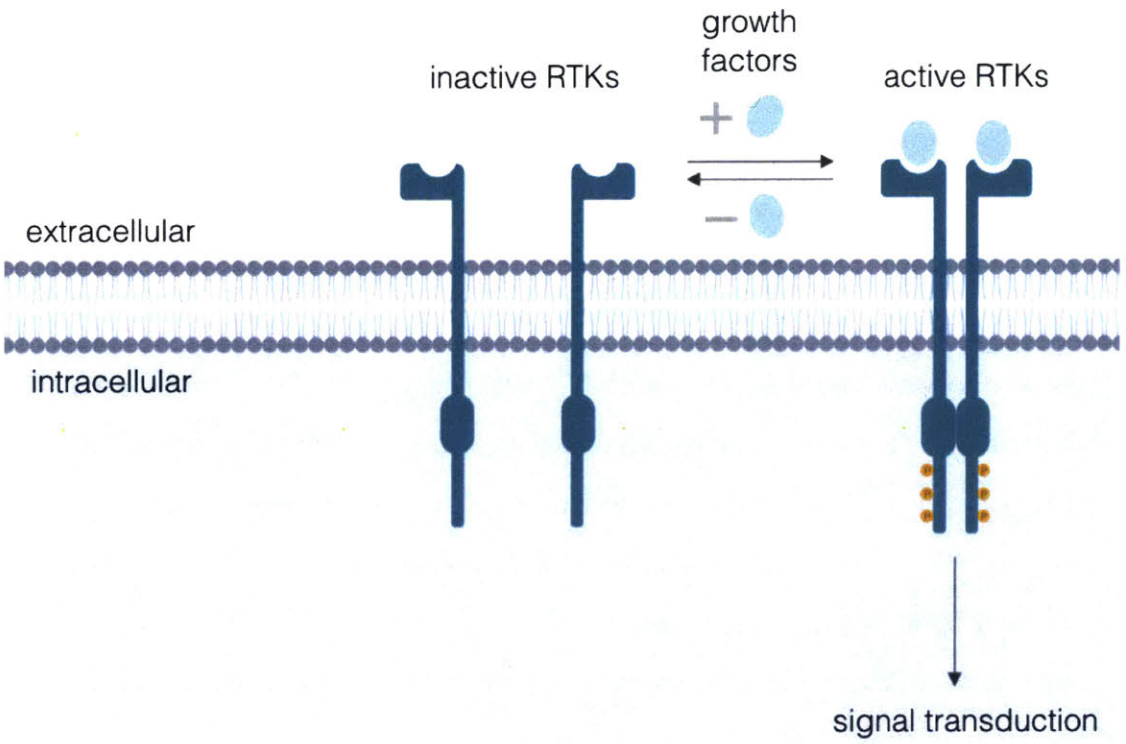

Figure 1-1: RTK-induced signal transduction.

Cell-surface RTKs bind extracellular growth factor ligands, leading to phosphorylation of their tyrosine kinase domains and subsequent signal transduction.

membrane-anchored pro-forms that are then cleaved by proteases to yield bioactive soluble factors in a process termed ectodomain shedding. [14] They may be derived from other cell types in the surrounding environment, or malignant cells can even upregulate their own growth via autocrine signaling loops, such as in the case of stem cell factor and the KIT proto-oncogene in small cell lung cancer. [15–17]

The specific growth factors with the greatest influence on a cancer's progression depends upon the specific RTK(s) driving its oncogene addiction. Accordingly, these dependencies can change if a tumor accumulates heterogeneous cell populations (subclones) as it progresses, or if it evolves to develop resistance following the administration of certain therapeutic regimens. For example, RNA

and protein upregulation of transforming growth factor alpha (TGFα) was detected in MET inhibitor-resistant clones of MET-addicted gastric cancer cell lines. [18] Additional experiments by the Engelman group showed that TGFα-dependent activation of EGFR was sufficient to promote resistance to MET inhibition. In a separate model of ALK inhibitor-resistant non-small cell lung cancer, increased levels of EGFR ligands such as amphiregulin, but not EGFR mutation or amplification, were found to be associated with persistent EGFR activation. [19] Finally, relative to parental cells, AXL and its ligand GAS6 were upregulated at the protein level in EGFR inhibitor-resistant clonal outgrowths of EGFR-mutant lung cancer. [20] Immunohistochemistry of paired patient specimens obtained at baseline and upon acquired resistance to the EGFR inhibitors erlotinib or gefinitib indicated that AXL and GAS6 overexpression were clinically relevant. Overall, studies such as these highlight the influence of extracellular signaling events on tumor cell RTK dependencies.

1.1.3 RTK-activated intracellular signal transduction pathways

Many of the proteins in signaling networks downstream of RTKs have been identified, including how activation of specific RTKs triggers changes in their abundance and signaling flux. Detailed biochemical experiments have elucidated crosstalk between signaling nodes, as well as positive and negative feedback mechanisms that may vary depending on protein expression and/or activity levels of pathway members. [21] Discussion of all possible permutations of these networks is not within the scope of this introduction, but a few signal transduction pathways most relevant to cancer are described here.

The phosphatidylinositol 3-kiase (PI3K) pathway, which activates the serine/threonine kinase AKT, is often dysregulated in cancer. Genetic loss of the lipid phosphatase PTEN confers susceptibility to many cancer types by removing

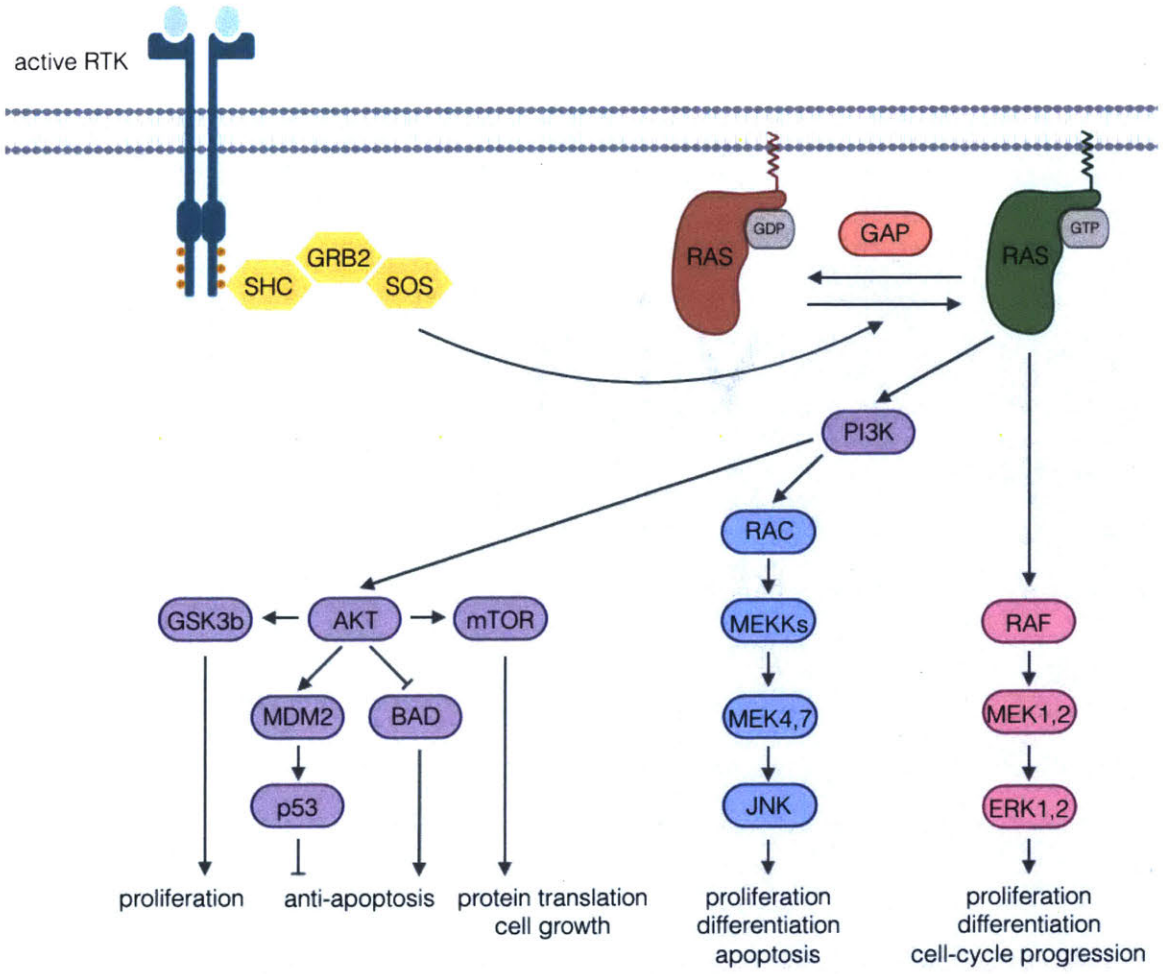

Figure 1-2: Major signaling pathways triggered by RTKs.

Figure adapted from [22]. Example of signaling pathways – including PI3K, JNK, ERK – activated by the receptor MET and leading to downstream cellular responses in cancer cells.

a suppressor of this pathway. [23] AKT then acts to promote proliferation by activating mTOR. Alternatively, protection from apoptosis is acquired via inactivation of the pro-apoptotic protein BAD, or via activation of the E3 ubiquitin-protein ligase MDM2, which promotes degradation of the pro-apoptotic (tumor suppressor) protein p53 (Fig. 1-2).

c-Jun NH_2-terminal kinase (JNK) is primarily activated in response to stress

and pro-inflammatory cytokines. [24] However, while conventionally referred to as a critical mediator of apoptosis in response to cellular stress, such as in neurons or embryonic fibroblasts during development, many studies have also shown that it can ablate the expression of anti-apoptotic genes and/or induce cell differentiation and growth.

The MAPK/ERK pathway discussed further in Section 1.2 is likely the most well-studied in cancer. It involves the successive activation of a chain of kinases (RAF, MEK, ERK) that culminates in translocation of ERK to the nucleus, where it phosphorylates a variety of transcription factors that normally regulate cell growth under conditions of homeostasis but can lead to transformation under conditions of overactive signaling.

These pathways are interconnected across many levels. Notably, activated RAS can actually activate PI3K, which can lead to signaling flux through the PI3K/AKT pathway or even activation of JNK signaling via the Rac GTPase. Another emergent theme across even just the few signaling pathways mentioned here lies in their context-dependence – for example, due to varying expression levels of pathway members, they can yield completely opposing cellular outcomes in different cell types. Because of this, systems biology approaches have been and will continue to be crucial for quantitatively understanding the complex architecture of signaling networks that are downstream of RTKs.

1.1.4 RTKs, upstream growth factors, and downstream intracellular kinases as therapeutic targets

Our knowledge of RTK-related signaling pathways began with an understanding of how they function and are regulated in normal physiological states. It then progressed towards investing how pathway checks and balances might be altered in different disease states. Because RTKs are often crucially involved in cancer development and progression, they are important targets for therapeutic intervention.

Drugs directly targeting RTKs fall into 2 main categories: 1) small molecule inhibitors known as tyrosine kinase inhibitors that target the intracellular kinase domain or 2) monoclonal antibodies that bind RTKs extracellularly. [1] Drugs targeting upstream growth factors often take the form of monoclonal antibodies raised against (portions of) the growth factors themselves or chimeric proteins in part comprised of an RTK's ligand-binding domain. Both drug classes act as soluble ligand traps by binding free ligand such that they become unavailable to activate cell-surface RTKs. In some cases, rational design and/or directed evolution have been applied towards engineering these soluble decoy receptors to be better binders of their growth factor targets, all while minimizing off-target binding. [25–27] Drugs targeting downstream intracellular kinases are small molecule inhibitors that either bind allosteric sites or are ATP-competitive. [28] These are largely hydrophobic and can therefore easily pass through the cell membrane, in contrast to monoclonal antibodies.

Each of the aforementioned drug categories have their own advantages and disadvantages. For example, while oral delivery of biologics is not possible due to the harsh environment of the digestive system, they are generally highly selective for their targets, with low potential of off-target effects. On the other hand, many tyrosine kinase inhibitors are referred to as "dirty" and can lead to unintended side effects via binding to heavily conserved RTK kinase domains. Furthermore, kinase inhibitors of intracellular proteins can possibly be more effective due to inhibition of downstream signaling nodes that many pathways converge onto. However, if the inhibitor is not highly specific for a mutant form of its target kinase only expressed in cancer cells, then healthy cells may be exceedingly vulnerable to inhibitor-induced killing, possibly leading to dose-limiting toxicities in the clinic. These characteristics of various targeted therapies will be important to keep in mind, as they will all be used at some point within this thesis either as therapeutic interventions or tool compounds to elucidate mechanism.

1.2 The mitogen-activated protein kinase (MAPK) pathway in cancer

1.2.1 MAPK hyperactivity

The canonical MAPK/ERK pathway plays a vital role in the regulation of gene expression, cellular growth, and survival. In this pathway, extracellular signals bind transmembrane glycoproteins known as receptor tyrosine kinases (RTKs), which upon phosphorylation of their intracellular tyrosine kinase domains, then recruit adaptor proteins that promote the conformation of RAS in its GTP-bound state. Activated RAS then transduces signal down the protein kinase cascade via the successive phosphorylation of RAF, MEK, and finally ERK. Phosphorylated ERK translocates into the nucleus, where it phosphorylates an array of targets to trigger a cellular response. Dysregulation of ERK signaling is associated with a broad array of cancers, and in many cases, it arises as a result of mutations in the kinases within the intracellular pathway and/or overexpression of upstream RTKs, ultimately leading to pathway hyperactivity and subsequent cancer cell proliferation and differentiation. [29]

Collaborative sequencing projects, such as The Cancer Genome Atlas (TCGA) and the Catalogue of Somatic Mutations in Cancer (COSMIC), have revealed that BRAF mutations are present in 7-15% of all cancers and highly prevalent in melanoma, as well as thyroid, colorectal, and ovarian cancers. [30,31] The V600E mutation accounts for approximately 90% of all mutations in BRAF and renders the kinase constitutively active, thereby enabling mutated cells to become self-sufficient even in the absence of external MAPK/ERK-activating stimuli. [32,33]

Additionally, RAS mutations are found in 16% of all cancers and most prevalent in those of the pancreas and colon, with KRAS being the most frequently

mutated isoform and the most commonly mutated oncogene overall. [34] Under normal signaling conditions, RAS is tightly regulated by guanine nucleotide exchange factors that promote GDP dissociation and GTP binding in order to turn on signaling, as well as GTPase-activating proteins that stimulate RAS' intrinsic GTPase activity in order to turn off signaling. Activating mutations impair the ability of RAS to hydrolyze GTP and therefore increase the likelihood that RAS remains in its active, GTP-bound state. Overall, this increases MAPK signaling flux though ERK, but signaling activity is still dependent on the presence of extracellular factors.

In cancers that possess more modest yet still significant mutation and copy number alteration rates, it is possible that MAPK/ERK signaling can also be dysregulated due to upregulated gene expression of canonical signaling pathway members. Notably, this is the case in type I ovarian tumors – comprised of the low grade serous, clear cell, mucinous, and endometrioid histological subtypes – which consistently rank near the very top when sorting by KRAS gene expression across all tissue types of cancer.

1.2.2 Targeting MAPK-mutant cancers

The frequency of aberrant MAPK/ERK activation across diverse cancer types has spurred extensive research and development of MAPK inhibitors (MAPKi). However, to date, the only currently approved MAPKi are the combinations encorafenib/binimetinib, dabrafenib/trametinib and vemurafenib/cobimetinib (BRAFi/MEKi) for $BRAF^{V600E/K}$-mutant melanoma, thyroid cancer, or non-small cell lung cancer patients. [35,36] In both settings, while initial responses are significant and approach 70% of treated patients, the median length of response lies below a year.

Moreover, although ATP-competitive RAF inhibitors have high specificity for cells with $BRAF^{V600}$ mutations, they are largely ineffective against and can even

paradoxically activate the MAPK pathway in RAS-mutant (BRAF wild-type, as these mutations are typically mutually exclusive) cancers. [37–42] Direct inhibition of RAS has been difficult due to its perceived lack of drug-binding pockets, although covalent $KRAS^{G12C}$-specific inhibitors have recently been discovered and have demonstrated activity in preclinical models. [43–45] First-in-human trials for $KRAS^{G12C}$ inhibitors have begun, but even if they are effective, these highly selective therapies would likely only be useful in a small population of patients with KRAS-mutant tumors.

Due to the elusiveness of targeting RAS directly, other approaches to inhibiting its function have been explored in recent years. These include exploring inhibitors of RAS-dependent metabolic processes such as macropinocytosis or autophagy. [46,47] Several research groups have also attempted to exploit synthetic lethal interactions by screening for genes essential to the maintenance of oncogenic growth in RAS-mutant cancers. [48] The main strategy, however, has been to directly inhibit downstream effector signaling by targeting MEK or ERK. [43] In the past few years, ERKi such as GDC-0994, MK-8353, and ulixertinib have begun to make headway; nevertheless, most work to date has focused on MEKi. [49–51]

Unsurprisingly, clinical trials of MEKi in MAPK-dysregulated tumors have produced lackluster results. Despite demonstrated activity against BRAF-mutant cancers, MEKi as monotherapies have shown only some activity in patients with NRAS-mutant melanoma, and have had little effect in those with KRAS-mutant cancers. [52] For example, a randomized phase II study of the non-ATP competitive, allosteric MEK1/2 inhibitor trametinib yielded only a 12% response rate in patients with KRAS-mutant advanced non-small cell lung cancer, faring no better than standard chemotherapeutic second-line therapy. [53] Additionally, a recent phase II trial of selumetinib in low-grade serous ovarian cancer (LGSOC) demonstrated a modest 21% tumor response rate uncorrelated with the presence of a BRAF or KRAS mutation. [54] Thus, there exists a clear need to investigate the resistance mechanisms underlying lack of initial and durable MAPKi response.

1.2.3 Tumor-intrinsic MAPKi resistance

Tumor cell-autonomous mechanisms of resistance to MAPK pathway inhibition have been extensively studied and are associated with MAPK reactivation and/or compensatory activation of other signaling pathways. They can arise as a result of genetic alterations, as well as protein-level changes, and have accordingly been profiled with the use of both genomic and proteomic techniques. [55] Several well-characterized examples are detailed here, although this is by no means an exhaustive list.

In one instance, based on whole-exome and whole-transcriptome sequencing of paired pre-treatment and progression BRAF-mutant melanoma tumor biopsies, MEK activating mutations were found to drive clinical acquired resistance to combined RAF/MEK inhibition. [56] Similar results, as well as secondary BRAF or RAS copy-number amplifications, have been shown following the use of various MAPKi across other MAPK-mutant cancers. [57–59]

On the level of the proteome, inhibition of MAPK signaling generally results in inhibition of the negative feedback mechanisms that are normally in place when the pathway is active. [60] This includes phosphoERK-mediated inhibitory phosphorylation of MEK and CRAF, DUSP-mediated ERK de-phosphorylation, and SPRY-mediated inhibition of adaptor protein recruitment in response to upstream RTK phosphorylation. [61–63] In addition to feedback reactivation, MAPKi can also lead to widespread transcriptional derepression of RTKs and cytokines that are normally held in check by ERK phosphorylation of the transcription factor c-Myc. [64] RTK upregulation can even be due to post-translational mechanisms, such as MAPKi-induced reduction of RTK ectodomain cleavage by metalloproteinases. [65] This extracellular proteomic rewiring enhances cell-surface RTK expression, particularly that of AXL and MET, and therefore increases the likelihood that bypass signaling, via pathways such as JNK or AKT, can circumvent cell death even in the presence of kinase inhibition.

1.2.4 Influence of the tumor microenvironment on MAPKi resistance

While expression of receptors connecting extracellular signals to intracellular kinases can be important in mediating drug resistance, abundance of the extracellular signals themselves can be just as crucial, as many RTKs only become activated once bound to their cognate ligands. Growth factors can be derived from tumor cells themselves, or can also be secreted or proteolytically shed from other cell types and subsequently interact with tumor cell RTKs in a paracrine fashion. A screen of over 40 kinase-addicted cell lines co-treated with appropriately matched kinase inhibitors and a panel of six RTK ligands (hepatocyte growth factor [HGF], epidermal growth factor [EGF], fibroblast growth factor [FGF], platelet-derived growth factor [PDGF], neuregulin 1 [NRG1], and insulin-like growth factor [IGF]) demonstrated a widespread potential for growth factor-driven rescue of inhibitor-induced cell killing. [66] In this screen, growth factors were exogenously added to cancer cell mono-cultures, showing that other cell sources of these ligands could yield a similar effect if co-cultured with cancer cells in vitro or if present within the tumor microenvironment.

Since then, many reports of activating ligands from neighboring cell types have been published. Fibroblast secretion of HGF was found to activate MET on nearby melanoma cells, leading to MAPK reactivation, PI3K/AKT activation, and ultimately resistance to the RAF inhibitor PLX4720. Along these lines, expression of stromal cell HGF was increased in BRAF-mutant melanoma patients who exhibited innate resistance to BRAFi. [67] Similarly, exogenous addition of NRG1 and HGF were shown to mediate MEKi resistance by activating AKT signaling after binding to their respective receptors, ERBB3 and MET. [68] These phenotypic effects were reproduced when conditioned media from fibroblast cell lines (that produced NRG1 and HGF) was added in place of purified ligand.

Other groups have focused on kinase inhibitors' immunomodulatory effects. For example, trametinib either alone or in combination with dabrafenib was found

to have deleterious effects on in vitro T cell proliferation and antigen-specific T cell activation. [69] However, different conclusions arose from separate studies, where longer-term in vitro experiments suggested that MEKi is only transiently immunosuppressive and actually acts to delay the kinetics of T cell activation and cytokine secretion. [70] Concurrent or sequential administration of trametinib with immune checkpoint blockade via an anti-PD-1 antibody was superior to either drug alone in a syngeneic model of CT26 KRAS-mutant mouse colorectal cancer. More extensive in vivo studies appeared to demonstrate that MEKi enhanced the presence of tumor-infiltrating, antigen-specific $CD8^+$ effector T cells by preventing exhaustive apoptosis, and synergized with an anti-PD-L1 antibody in the same CT26 model. [71] Despite these promising preclinical studies, IMblaze370 – a phase 3 trial comparing atezolizumab (an anti-PD-L1 antibody) +/- cobimetinib (MEKi) versus regorafenib (a multikinase inhibitor) in metastatic colorectal cancer – did not meet its primary endpoint of improved overall survival. [72] These results suggest that there may be deleterious effects potentiated by MEKi in cell populations within immunologically cold tumors, such as myeloid or regulatory T cells, that had not been taken into account.

Taken together, these studies highlight the importance of considering a therapy's impact on the tumor microenvironment, as well as its subsequent effect on intercellular signaling cascades, when investigating drug resistance.

1.3 Overview and scope of thesis work

This thesis work aims to improve our understanding of the contribution of and mechanisms underlying cell-cell communication in MAPKi resistance. We focus on MAPK-mutant melanoma and primarily ovarian cancer as model systems, as they are two tissue types of cancer that demonstrate either intrinsic or adaptive resistance to MAPKi, as shown through prior clinical trials.

In Chapter 2, we describe the use of computational methods to generate testable hypotheses on the association of the tumor microenvironment with drug response. We first apply a deconvolution algorithm towards publicly available, matched patient gene expression data to identify immune cell populations that might be correlated with MAPKi resistance. We next use single-cell or bulk RNA sequencing of patient samples to quantify over 1,000 intercellular receptor-ligand interactions between all possible pairs of cancer cells and stromal or immune cell populations. These analyses suggest that increases in macrophage populations are associated with increased MAPKi-treated patient tumor burden and that there exists enriched signaling between cancer cells and tumor-associated macrophages (TAMs) via the receptor tyrosine kinase MET with its cognate ligand HGF, as well as AXL and MERTK with GAS6. These specific RTKs have previously been implicated, by our group and others, in tumor-intrinsic resistance pathways across various cancer types.

In Chapter 3, we focus on acquiring a systems-level understanding of TAM-tumor crosstalk contributions to MAPKi resistance. We employ multiplex proteomic measurements of cytokines, growth factors, RTKs, and intracellular kinases from TAMs and cancer cell lines grown in mono- and co-culture models. This is done with the aims of understanding not only how MAPKi impacts TAM and cancer cell signaling individually, but also how MAPKi influences cancer cells' effects on TAMs, and vice versa. Most notably, we find that attenuated decreases in tumor cell JNK signaling are associated with increases in macrophage-supplied growth factors and increased cell viability in the presence of MAPKi. To assess whether the signaling changes we observe in vitro are relevant in an in vivo tumor microenvironment, we develop an intravital imaging approach to simultaneously monitor single-cell kinase activities in real-time following MAPKi treatment. Using this strategy, we discover that MAPKi elicits increased TAM accumulation, and that these TAMs do in fact locally impact tumor cell signaling.

Finally, in Chapter 4, we develop a translational strategy to therapeutically

exploit reciprocal bypass signaling for overcoming resistance. We take into account our in vitro signaling measurements to rationally identify pharmacological perturbations that are synergistic with MAPKi, and in turn assess the impact of combination therapy on bypass RTK signaling in both TAMs and tumor cells. We optimize the nano-formulation of a previously developed multikinase inhibitor in order to selectively target TAMs, especially when co-treated with MAPKi, and extend survival in a mouse model of intraperitoneally disseminated ovarian cancer.

Overall, this thesis presents a framework for understanding multicellular networks of drug resistance and developing therapeutic strategies to target them.

2 Cellular and molecular contributions to MAPKi response

2.1 Introduction

Most work to date has either examined cancer cell-autonomous resistance, or has been very targeted in examining intercellular interactions between specific cell types within the tumor microenvironment. A systematic approach to test all ligand-receptor pairs, across all interacting pairs of cell types in a tumor, would aid in understanding signals associated with phenotypic responses of interest.

In this chapter, we focus on the computational analysis of previously published gene expression data to derive testable hypotheses. We first apply a deconvolution algorithm known as CIBERSORT to determine if there are certain immune cell populations that might correlate with tumor progression in a small cohort of BRAF-mutant metastatic melanoma patients treated with dabrafenib and trametinib combination therapy. Beyond characterizing cellular composition as correlates of disease progression, we then perform a ligand-receptor interaction analysis on a separate, single-cell RNAseq data set profiling over 4500 immune and non-immune cells from 19 melanoma patient tumors, with the aim of identifying pairwise growth factor-RTK interactions that might be enriched at the RNA level.

To assess whether our findings might also be relevant in another tissue type of MAPK-mutant disease, we then profile the cellular composition of a larger group of ovarian tumor biopsies acquired from primary debulking surgery. Ligand-

receptor interaction analysis on bulk gene expression data of sorted tumor epithelial cells, as well as immune cells from patient ascites, highlights intercellular cross-talk predicted to be present in both model systems.

2.2 Results

2.2.1 TAM presence correlates with increase in MAPKi-treated patients' melanoma tumor burden

CIBERSORT deconvolution takes in bulk transcriptional profiles of samples and, using reference gene matrices of 22 different purified leukocyte populations, infers the relative immune cell proportions that make up each sample. [73] We applied this method towards a data set comprised of 20 $BRAF^{V600}$-mutant melanoma metastases derived from 10 patients treated with dabrafenib/trametinib. [74] Bulk sequencing data was obtained from each patient prior to MAPKi initiation and upon progression, and the same site (subcutaneous, bowel, peritoneum, or omentum) was biopsied at each time point. Importantly, the availability of Response Evaluation Criteria in Solid Tumors (RECIST) data enabled us to determine correlations with clinical outcomes.

Monocyte and macrophage subpopulations, resting mast cells, follicular helper T cells, and $CD8^+$ T cells were found to, on average, comprise the largest immune cell fractions across all 20 metastases (Fig. 2-1). When considering individual immune populations, only an increase in naïve B cells was significantly correlated with an increase in tumor burden (Spearman $r = 0.66$) (Fig. 2-2A). This stemmed from the fact that naïve B cells were either minimally or not at all present in pre-treatment samples of patients classified as having stable disease (Fig. 2-1). While an increase in M0 and M2 macrophages only moderately individually correlated with worse patient response, the linear combinations of M0 + M1 + M2

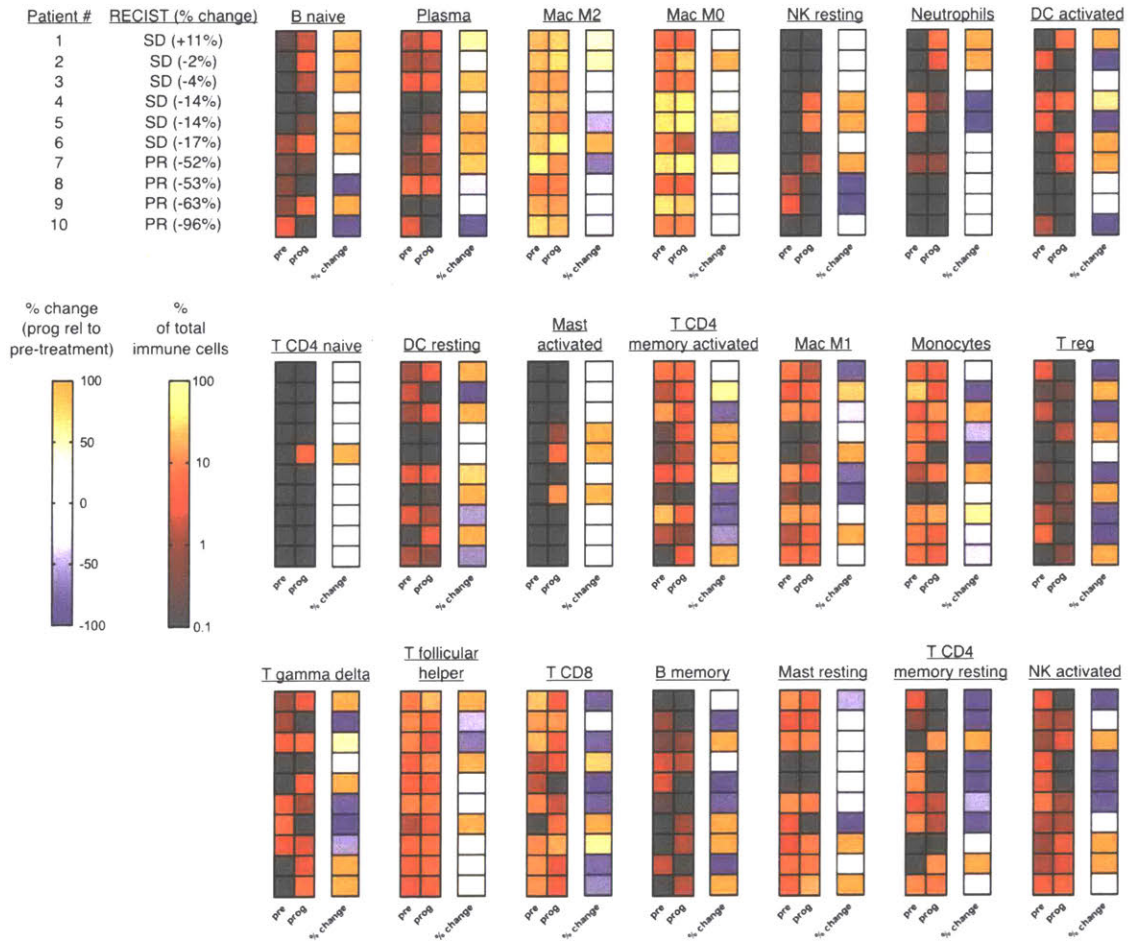

Figure 2-1: Inferred immune cell proportions from MAPKi-treated melanoma patient samples.

Pre-treatment and progression levels of each immune cell type, as well as their % change, are shown for each patient. Patients were ranked by % change in tumor size (SD = stable disease, PR = partial response). Eosinophils were not inferred to be present in any of the 20 samples, and are therefore not shown on this heat map.

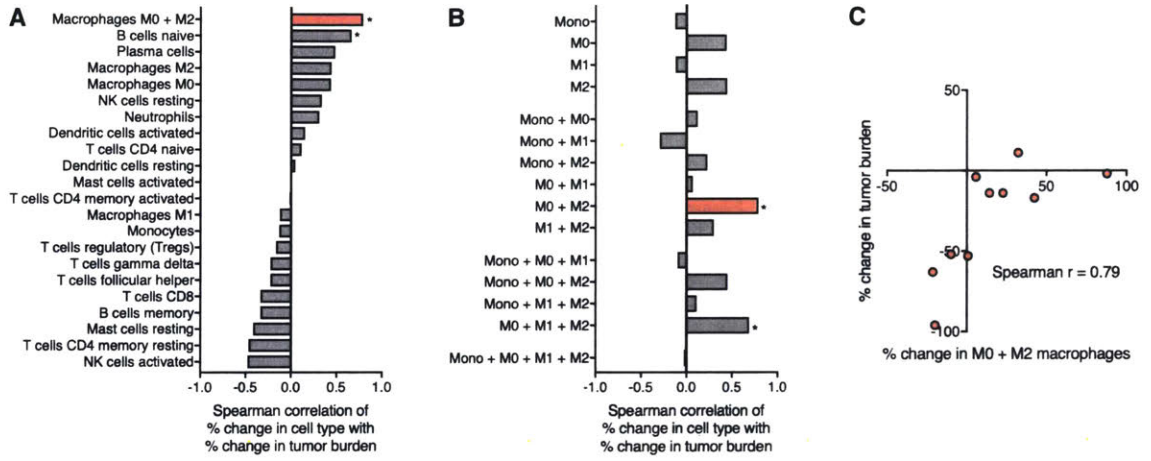

Figure 2-2: Immune cell correlates of melanoma patient tumor burden following MAPKi.

(A) Spearman correlation of % change in relative immune cell fractions with % change in tumor burden. Individual populations are ranked from most positively to most negatively correlated, with the overall most significantly correlated M0 + M2 macrophage subsets added for reference (*$p < 0.05$). (B) Same as (A), except with all possible linear combinations of monocyte and macrophage subsets. (C) Individual data points for the most significantly correlated subpopulation ($p = 0.009$).

macrophages (Spearman r = 0.69) and especially of M0 + M2 macrophages (Spearman r = 0.79) were significantly predictive (Fig. 2-2B-C). Further analysis indicated that partial responders did not have lower pre-treatment macrophage amounts (data not shown), demonstrating that only changes in relative macrophage fraction, as opposed to the initial levels, were associated with clinical outcome.

2.2.2 Macrophage-supplied growth factors possibly amplify melanoma cell RTK signaling

To identify intercellular signaling pathways that might be present amongst cell populations of interest, we performed ligand-receptor interaction analysis as detailed in [75] on a single-cell RNA sequencing (scRNA-seq) data set comprised of over 4500 immune ($CD45^+$) and non-immune ($CD45^-$, including malignant and

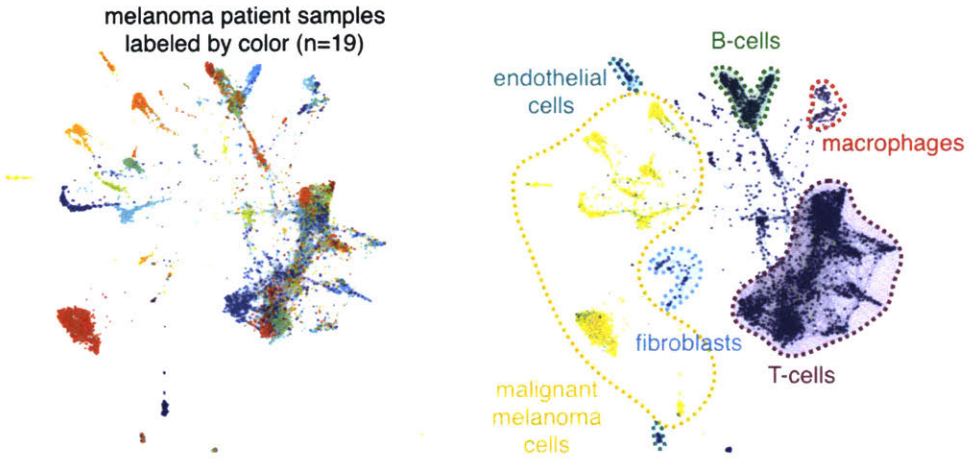

Figure 2-3: SPRING visualization of melanoma patient scRNAseq data.

Clusters of malignant melanoma, immune, and stromal cells were visualized using cell-type specific markers defined in the Tirosh et al. publication.

stromal) cells from 19 malignant melanoma patients. [76] The sample set consisted of NRAS-mutant, BRAF-mutant, and wildtype tumors from various metastatic sites, and some patients received prior treatment while others were treatment-naïve. Although our focus lies on MAPK-mutant disease, due to the limited cell numbers from any one tumor, all cells were analyzed in this analysis. Cell-type classification based on pre-defined markers from the original publication yielded distinct clusters in k-nearest-neighbor SPRING plots (Fig. 2-3). [77]

Autocrine and paracrine ligand-receptor interactions – between all possible sender cells acting as ligand sources and all possible receiver cells expressing associated receptors – were quantified. For a given interaction, an interaction score was calculated by taking the product of average ligand expression across all sender cells and the average receptor expression across all receiver cells. In total, 1,180 known and literature-supported interactions, including those from chemokine, cytokine, and RTK families, were considered. [75,78,79] Here we focus on potential

tumor-macrophage interactions, due to the correlation of increasing macrophage abundance with disease progression. Additionally, we filtered for roughly 200 growth factor-RTK interactions, because tumor cells and macrophages are known to highly express both. Of the highest-ranking interaction scores, GAS6 primarily from macrophages possibly interacts with macrophage AXL and MERTK, and CSF1 from both cell types with macrophage CSF1R (Fig. 2-4). As AXL, MERTK, CSF1R are associated with macrophages' ability to suppress pro-inflammatory anti-tumor responses, this corroborates prior literature demonstrating that tumors themselves are able to shift their surrounding microenvironment into a pro-tumorigenic phenotype. [80,81] Additionally, a large amount of high interaction scores is evident when macrophages act as sender cells and tumor cells serve as receivers, suggesting that macrophages can in turn supply growth factors to amplify basal levels of tumor cell RTK signaling. Included in the top hits are the GAS6-AXL/MERTK and HGF-MET signaling axes, and this is particularly interesting because upregulation of these RTKs have previously been implicated in kinase inhibitor resistance across various cancers. [65,67,82]

2.2.3 MAPK-dysregulated ovarian cancer is enriched in macrophages at baseline

Following, we hoped to assess whether our previous findings were generalizable to MAPK-mutant cancer in a different tissue context. CIBERSORT deconvolution of microarray data from 90 ovarian primary tumor biopsies indicated that monocytes and macrophages were by far the most abundant immune cell types, and that MAPK-mutant tumors possessed a greater relative fraction of them (Fig. 2-5). [83] Reassuringly, this data set captured the high rate of MAPK mutations (here, mainly in KRAS or BRAF, with a few in ERBB2) characteristic of low-grade serous tumors, which are also known to be poor responders to traditional chemotherapy. However, because LGSOC is considered a rare tumor, there do not yet exist any published data sets of human ovarian tumors biopsied pre- and post-MAPKi. [84]

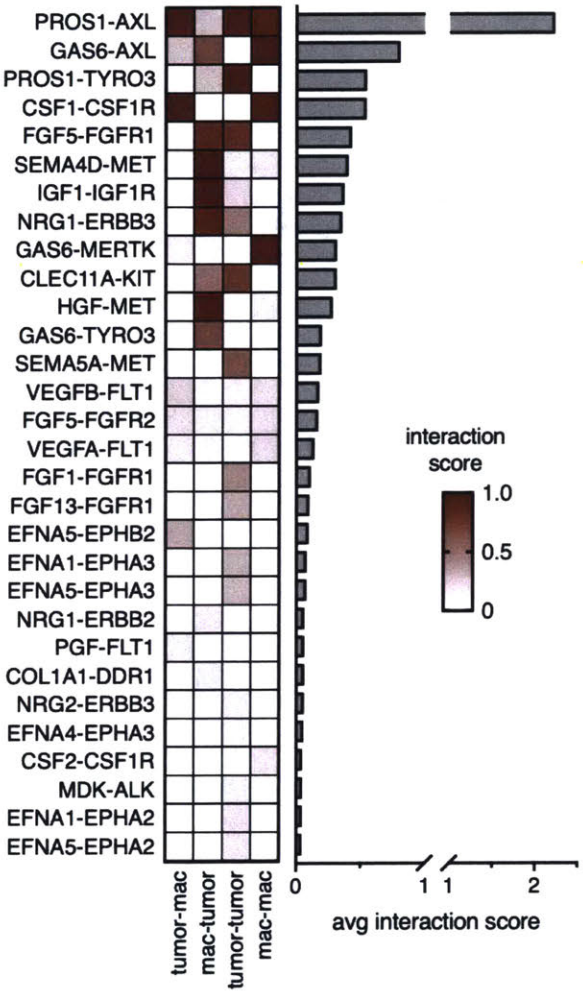

Figure 2-4: Top-scoring melanoma ligand-receptor interactions.

Top 15% interaction scores after filtering scRNAseq data for potential growth factor-RTK interactions, as well as tumor-macrophage autocrine and paracrine communication.

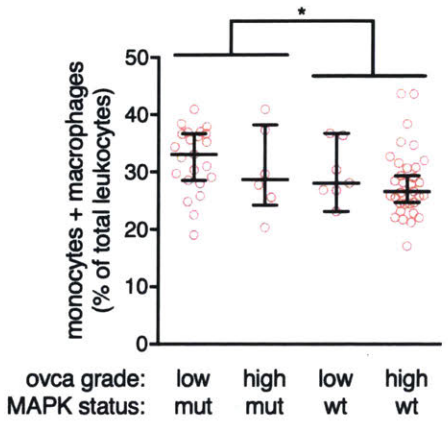

Figure 2-5: Inferred monocyte and macrophage proportions from ovarian tumor biopsies.

CIBERSORT deconvolution was performed on tumor biopsies from 90 ovarian cancer patients with either low- or high-grade, MAPK-mutant or wild-type disease. (*$p < 0.05$, two-tailed Mann-Whitney U test).

Therefore, while we can infer the presence of myeloid populations at the time of patient primary debulking surgery, we cannot yet deduce how their levels might be altered upon MAPKi.

2.2.4 LGSOC patient samples highly express RTKs and growth factors associated with known MAPKi resistance mechanisms

The limited LGSOC patient population likely also contributes to the unavailability of scRNA-seq data for this disease. Bulk microarray data of sorted cell populations were therefore used instead, and the ligand-receptor interaction analysis was adapted to enable comparison of expression values from different microarray platforms. We found two relevant data sets for the quantification of intercellular interactions: one containing sequencing of $CD16^{+}BDCA1^{-}$ macrophages isolated from the ascites (excess peritoneal fluid) of 5 untreated ovarian cancer patients,

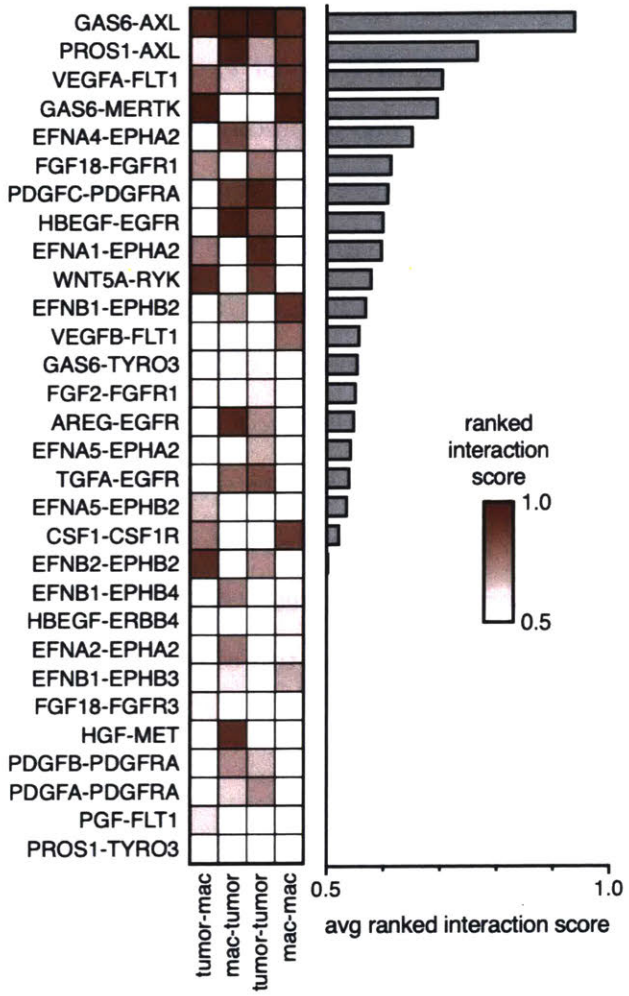

Figure 2-6: Top-scoring LGSOC ligand-receptor interactions.

To quantify potential intercellular growth factor-RTK interactions, bulk expression data of tumor epithelial cells sorted from LGSOC patient primary tumors, metastases, and ascites were used in combination with that of macrophages sorted from patient ascites. Top 15% ranked interaction scores are displayed.

and another with sequencing of 9 sorted EpCAM$^+$ tumor epithelial cell samples from primary tumors, metastases, and ascites of 3 LGSOC patients. [85,86]

For each interaction, a ranked (as opposed to absolute) interaction score was calculated by multiplying the average rank of ligand expression across all sender cells with the average rank of receptor expression across all receiver cells. Again, our reference interaction list was filtered down to roughly 200 growth factor-RTK pairs. Scores generated from expression data of primary tumors, metastases, and ascites were highly correlated (Pearson $r > 0.9$ in all cases, data not shown), and were therefore averaged into a single aggregate tumor score.

In comparison to the melanoma scRNA-seq analysis, higher-scoring interactions were not dominated by those involving macrophages acting as sources of ligands for tumor cells (Fig. 2-6). Instead, the directionality of signaling appeared evenly spread out across all 4 possible autocrine and paracrine pairings. Nevertheless, potential interactions between AXL/MERTK and their ligands GAS6/PROS1 once again appeared at the top of our ranked list.

2.3 Discussion

In this chapter, we employed previously developed computational approaches – namely, CIBERSORT and ligand-receptor interaction analysis – to generate testable hypotheses on the immune cell correlates of MAPKi resistance and the growth factor-RTK signaling pathways that may be involved. In malignant melanoma and LGSOC, our analyses suggest that macrophages are present in high abundance and that, at baseline, reciprocal signaling between macrophages and tumor cells may occur via the GAS6-AXL/MERTK and HGF-MET signaling axes, among others.

Our limitations lie primarily in the lack of extensive publicly available sequencing data. While the data sets we worked with were no easy feats for their

original publishers to acquire, it would be ideal to have data corresponding to the cancer mutational statuses and treatments relevant to the scientific questions at hand. Hopefully, this will be possible once improved experimental pipelines arise for processing biopsies into single cells and once patient tumor sequencing becomes even more readily integrated into clinical practice. Nevertheless, our results align with previous reports demonstrating the influence of stromal and immune cells within the microenvironment on tumor cell signaling. Our analysis further highlights the importance of considering bidirectionality of signaling when assessing the impact of therapeutics on a diseased state.

While our focus was on macrophages due to their perceived correlation with MAPKi resistance, the methodologies employed here are applicable to a wide variety of diseases and cell types, as long as the proper sequencing data is available to use as input. For example, we also found that increased ovarian cancer staging (stage III, IV vs. I, II) was associated with lower amounts of activated $CD4^+$ memory T cells and more regulatory T cells (data not shown). In this case, a broad analysis of interactions between these T cell subsets and other cell types within ovarian tumors could yield hypotheses for rationally designing combination therapies with immune checkpoint blockade.

2.4 Materials and methods

CIBERSORT analysis of patient samples. CIBERSORT uses a reference gene signature of roughly 550 differentially expressed genes from 22 leukocyte types to estimate the relative fraction of each within bulk transcriptional profiles of samples. [73] We applied this deconvolution algorithm to data sets accessed on the NCBI Gene Expression Omnibus (GEO): GSE61992, GSE12172. [74,83]

Ligand-receptor interaction analysis. Ligand-receptor interaction analysis of the scRNA-seq data from GSE72056 was performed as described in [75]. [76] Briefly,

each ligand-receptor interaction between cell type A and cell type B was scored as the product of average receptor expression across all A cells and the average ligand expression across all B cells. The reference list of known and literature-supported interactions was obtained from [78,79] and then annotated for growth factor-RTK interactions. Ligand-receptor interaction analysis of the bulk RNA expression data from GSE40484 and GSE73091 was performed similarly, with the exception that the ranks of ligand and receptor expression were used in place of absolute values. [85,86]

3 Tumor-macrophage crosstalk in MAPKi resistance

3.1 Introduction

The previous chapter featured analysis enabling us to predict the correlation of macrophage infiltration with drug resistance and the impact of specific macrophage-tumor growth factor-RTK interactions on previously elucidated tumor-intrinsic resistance mechanisms. These predictions only represent potential interactions because they were developed with the use of gene, as opposed to protein-level, expression data and do not take into account the spatial requirements of intercellular signaling within tumors.

In this chapter, we aim to experimentally validate our computationally generated hypotheses in various model systems. We hope to assess whether ligand-receptor interactions between cell types of interest are present at baseline, as well as whether they might be altered as a result of MAPKi. Namely, we enlist the use of multiplex proteomic measurements, in vitro co-culture systems, and in vivo confocal microscopy strategies to perform a systems-level dissection of microenvironment-mediated bypass signaling. We focus primarily on MAPK-mutant ovarian cancer, as targeted therapies for this disease subtype are particularly limited, and on the use of trametinib, as it is has been approved in other cancers and is currently being evaluated in a randomized phase II/III trial for recurrent ovarian or peritoneal cavity cancer (NCT02101788).

3.2 Results

3.2.1 Trametinib increases macrophage infiltration in mouse models of ovarian cancer via CCL5

To assess the presence of macrophages in mouse models of intraperitoneally disseminated ovarian cancer, we transfected two BRAF-mutant human ovarian cancer cell lines (ES2 and ptD patient-derived xenograft) with fluorescent reporters prior to i.p. inoculation in nu/nu mice. I.v. injection of fluorescent macrin 24 hr prior to sacrifice, followed by ex vivo imaging of harvested i.p. tumors, demonstrated the presence of TAMs in both models (Fig. 3-1). Treatment of mice with 3 daily oral doses of 0.3 mg/kg trametinib significantly enhanced macrophage infiltration.

To evaluate the kinetics of macrophage infiltration, we implanted the same ES2 cells as xenografts embedded in dorsal skin-fold window chambers. Daily longitudinal intravital imaging demonstrated unchanged macrophage presence within and outside the tumor boundary in vehicle-treated nu/nu mice (Fig. 3-2). In contrast, daily trametinib administration led to significant increases in macrophage recruitment, primarily localized outside the tumor periphery. Enhanced infiltration was evident not only compared to the control group tumors, but also relative to baseline levels by t = 72 hr.

We next sought to understand what factors might result in macrophage localization to the tumor site upon MEKi. We cultured ES2 cells, along with MAPK-dysregulated OVCA429 and KRAS-mutant OVCAR8 cells, in vitro for 24 hr with or without the presence of 100 nM trametinib. Luminex, a multiplex bead-based immunoassay, was then used to measure supernatant levels of a panel of 27 cytokines (Fig. 3-3A). RANTES (CCL5) – a chemotactic cytokine that binds CCR5 and is known to attract macrophages, T cells, eosinophils, and basophils – was the most highly upregulated following MEKi in all 3 cell lines. Accordingly, co-

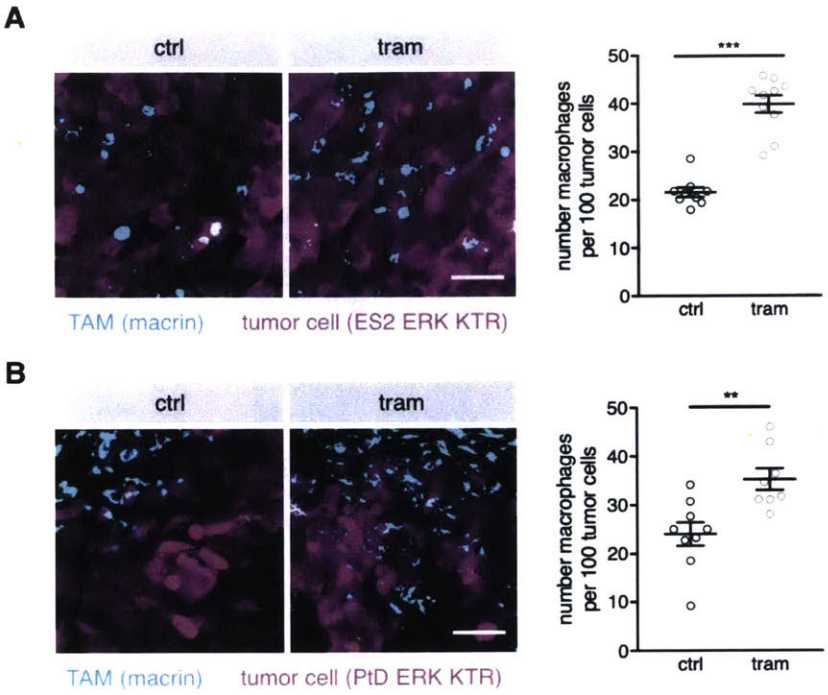

Figure 3-1: Trametinib-induced macrophage infiltration in mouse models of intraperitonally disseminated human ovarian cancer.

(A) Representative images and quantification of fluorescently labeled ES2 cells and TAMs within i.p. tumors excised 24 hr after 3 daily doses of oral vehicle or trametinib treatment. Multiple tumors from n = 3 nu/nu mice per group (***p < 0.001, two-tailed t-test). Scale bar: 50 μm. (B) Same as (A), except with ptD cells (**p < 0.01, two-tailed t-test).

treatment of nu/nu mice possessing i.p ES2 tumors with maraviroc (mvc, a negative allosteric modulator of CCR5 currently approved for treating HIV infection) attenuated trametinib-induced macrophage infiltration (Fig. 3-3B).

3.2.2 Macrophage depletion does not enhance trametinib efficacy in ES2 mouse model

Because TAM numbers increased as a result of MEKi, we next wanted to assess whether macrophage depletion might affect trametinib efficacy in the same model of i.p. ES2 disease. I.p. administration of clodronate liposomes every 3 days

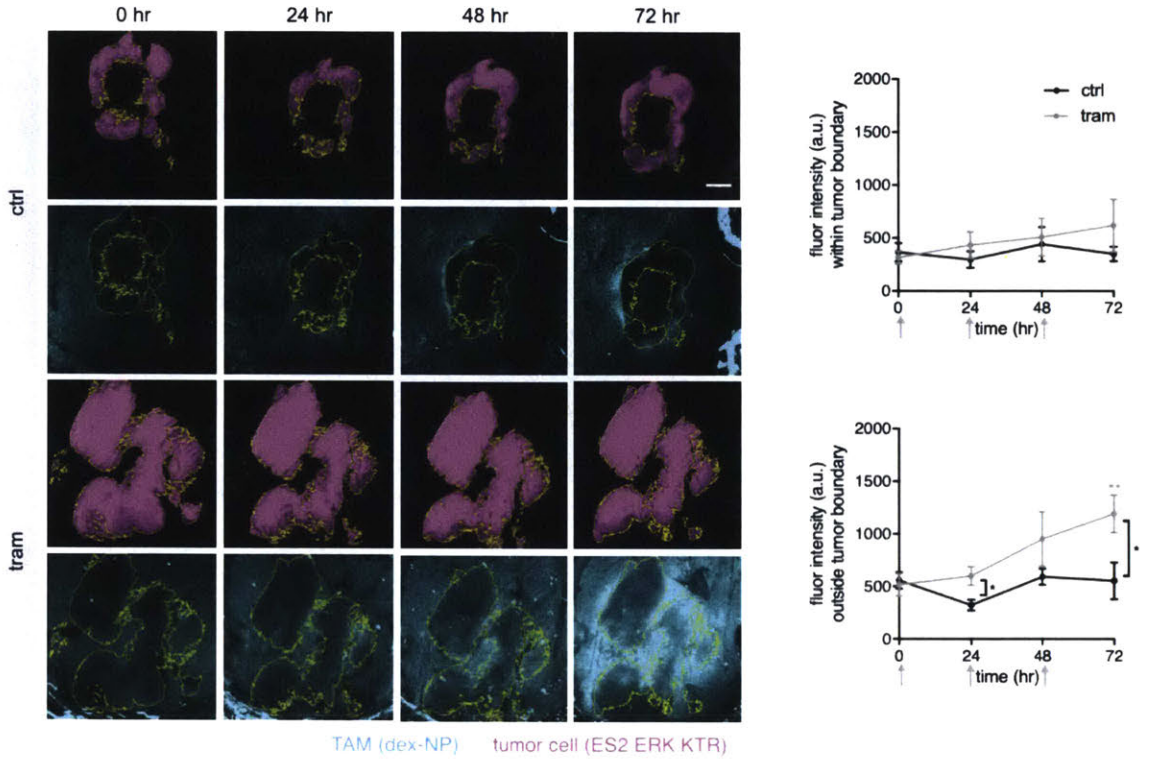

Figure 3-2: Longitudinal, trametinib-induced macrophage infiltration in xenograft model of human ovarian cancer.

(A) Representative longitudinal images and quantification of fluorescently labeled ES2 cells and TAMs within xenograft tumors grown in dorsal skin-fold window. Mice were treated daily with oral vehicle or trametinib. n ≥ 4 nu/nu mice per group. (gray **p < 0.01, two-tailed t-test compared to initial time point; *p < 0.05, two-tailed t-test comparing groups). Scale bar: 1 mm.

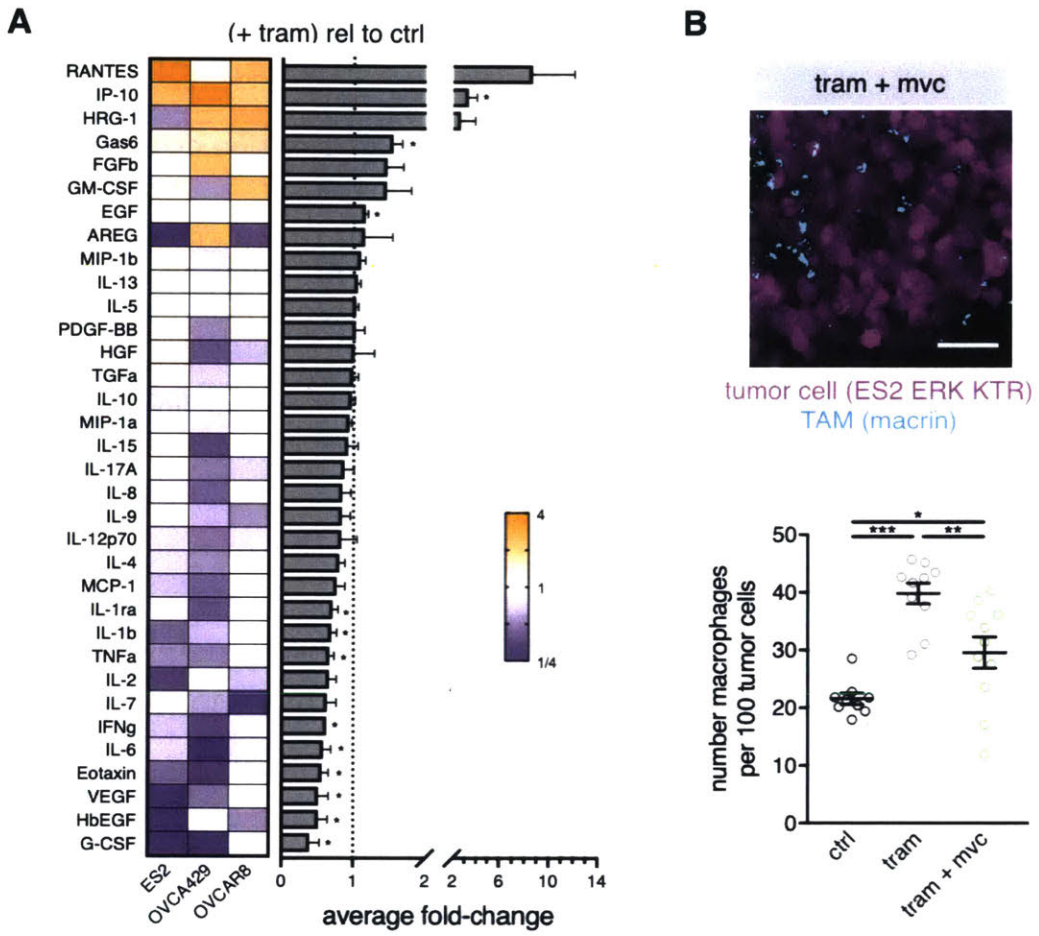

Figure 3-3: Ovarian cancer-secreted CCL5 recruits macrophages upon trametinib administration.

(A) Heat map depicting supernatant levels of cytokines (rows) produced by ovarian cancer cell lines (columns) 24 hr following trametinib treatment, as measured by Luminex. Ranked from highest to lowest average fold-change (*$p < 0.05$, two-tailed t-test). (B) Representative image and quantification of fluorescently labeled ES2 cells and TAMs within i.p. tumors excised 24 hr after oral trametinib + maraviroc (mvc) treatment. Multiple tumors from n = 3 nu/nu mice per group. Control and trametinib groups reproduced from Fig. 3-1A for comparison (*$p < 0.05$, **$p < 0.01$, ***$p < 0.001$, two-tailed t-test). Scale bar: 50 μm.

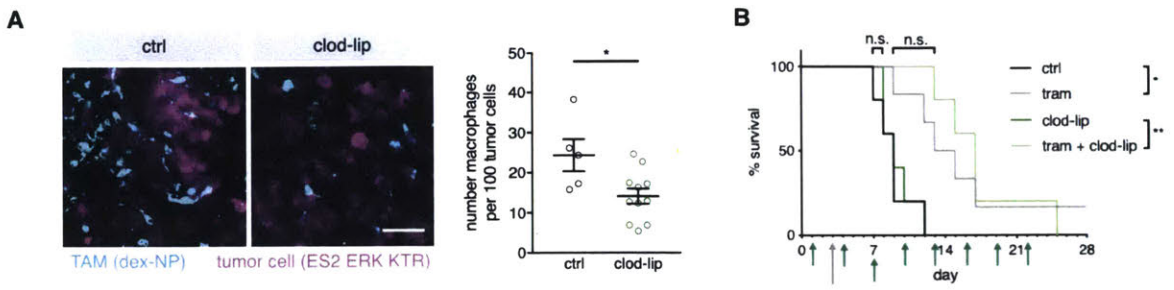

Figure 3-4: Clodronate liposome-mediated macrophage depletion does not enhance trametinib efficacy.

(A) Representative images and quantification of fluorescently labeled ES2 cells and TAMs within i.p. tumors excised following survival endpoint. (***$p < 0.001$, two-tailed t-test). Multiple tumors from n = 3 nu/nu mice per group. Scale bar: 50 μm. (B) Kaplan-Meier survival curves of nu/nu mice with ES2 i.p. tumors treated with trametinib, clodronate liposomes, or the combination. Large gray arrow denotes beginning of daily trametinib administration, while smaller green arrows denote control or clodronate liposome injection time points. $n \geq 5$ nu/nu mice per group (*$p < 0.05$, **$p < 0.01$, log-rank test).

effectively depleted TAMs (Fig. 3-4A), but neither improved overall survival nor significantly enhanced trametinib efficacy (Fig. 3-4B). Antibody-mediated macrophage depletion with i.p. injections of α-CSF1R yielded similar results (Fig. 3-5A). However, co-treatment with α-CSF1R did slightly reduce ascites volume (Fig. 3-5B) and significantly reduce ovarian tumor burden (as measured by excised ovary weights, Fig. 3-5C,D) in mice with comparable survival times.

3.2.3 Trametinib alters macrophage RTK signaling and function

In vitro measurements of M1- (classically activated, anti-tumor) and M2-polarized (alternatively activated, pro-tumor) U937 monocytic cell line-derived macrophages demonstrated that trametinib significantly enhanced CSF1R expression in both macrophage types (Fig. 3-6A,B), suggesting that α-CSF1R-mediated macrophage depletion may have not had a significant effect on survival (Fig. 3-5A) due to

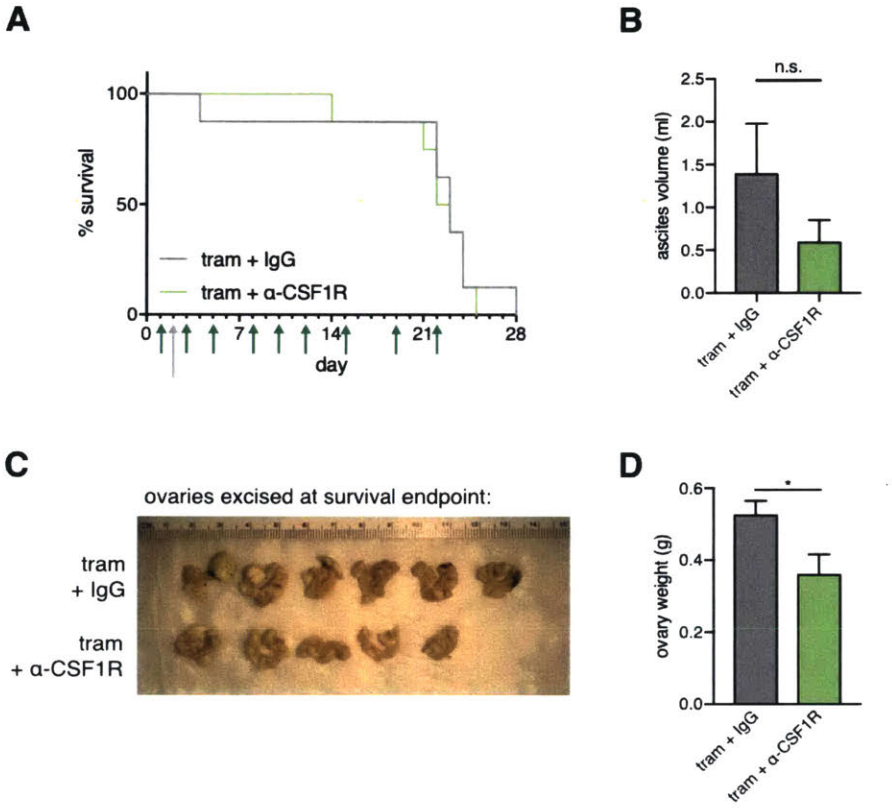

Figure 3-5: Impact of α-CSF1R antibody-mediated macrophage depletion on trametinib efficacy.

(A) Survival of mice with ES2 i.p. tumors and treated with trametinib + α-CSF1R antibody or IgG2a isotype control. Large gray arrow denotes beginning of daily trametinib administration, while smaller green arrows denote antibody injection time points. n = 8 nu/nu mice per group. (B-D) Ascites volumes and excised ovary weights at survival endpoints. n ≥ 5 mice with similar survival times per group (*p < 0.05, two-tailed t-test).

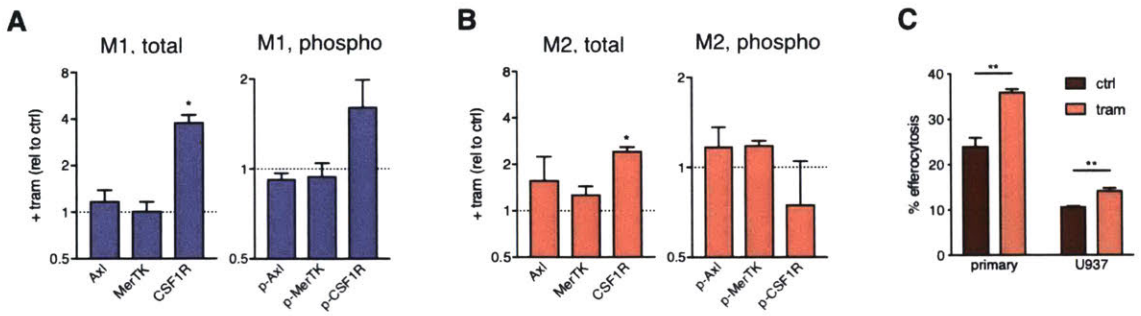

Figure 3-6: Trametinib alters macrophage RTK signaling and efferocytosis.

(A,B) Total and phosphorylated RTK levels of M1- and M2-polarized U937-derived macrophages 24 hr after trametinib administration, as measured by Luminex. (C) % efferocytic M2-polarized primary monocyte-derived or U937-derived macrophages +/- trametinib (*$p < 0.05$, **$p < 0.01$, two-tailed t-test compared to control).

simultaneous depletion of M1-polarized macrophages.

Trametinib also induced slight increases in AXL and MERTK expression and activity (Fig. 3-6B), leading us to believe that inhibition of MAPK/ERK signaling may exert possible influences on efferocytosis. Efferocytosis, the process by which apoptotic cell material is ingested and therefore removed by phagocytic cells, has been shown to be mediated primarily by MERTK and in part by AXL. [87,88] To test this functional consequence of MEKi, we first generated fluorescent apoptotic bodies by treating CellTracker Deep Red-labeled ES2 cells with high concentrations (10 mM) of trametinib for 48 hr. We then incubated these apoptotic bodies with pre-treated M2-polarized primary monocyte- or U937-derived macrophages for 4 hr, and assessed their efferocytic capabilities by gating for Deep Red^+ macrophages following flow cytometry analysis. As expected, at baseline, primary macrophages possessed greater functional capacity for efferocytosis than those derived from a monocyte cell line (Fig. 3-6C). Interestingly, treatment with trametinib predisposed macrophages from both cell sources to engulf greater amounts of tumor cell apoptotic material, suggesting that MEKi can promote macrophage wound-healing properties.

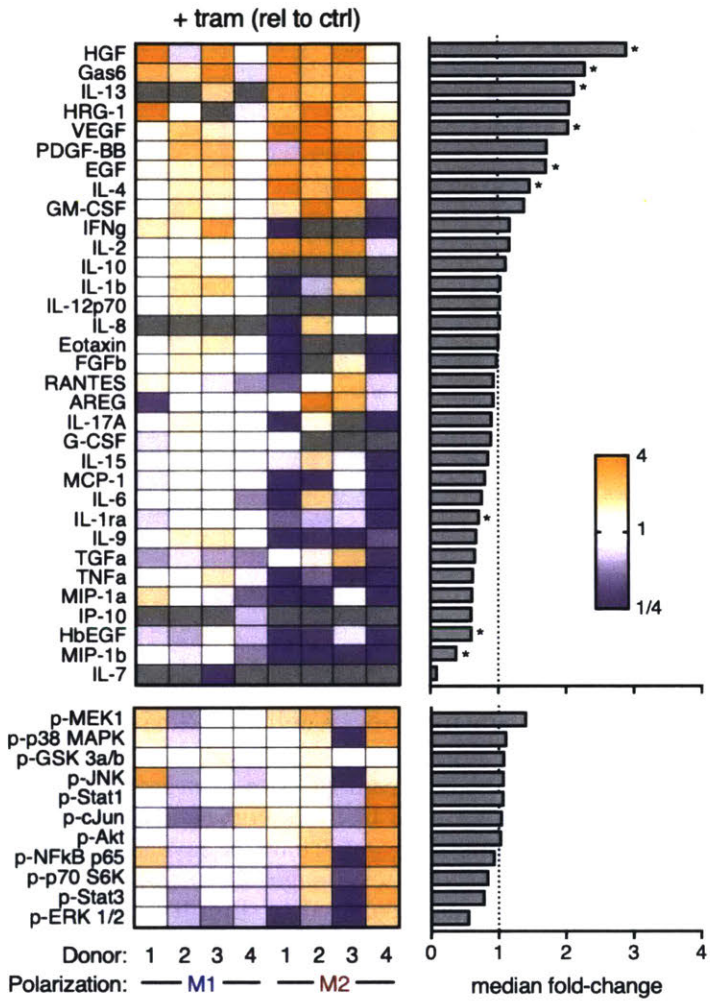

Figure 3-7: Trametinib alters levels of macrophage growth factors, cytokines, and active intracellular kinases.

Heat map depicting supernatant levels of growth factors and cytokines (rows) associated with primary monocyte-derived macrophages 24 hr following trametinib treatment, as measured by Luminex. Lysate levels of phosphorylated kinases are also shown (rows). Monocytes were isolated from the blood of 4 healthy donors (columns). Ranked from highest to lowest median fold-change (*$p < 0.05$, two-tailed Mann Whitney U-test).

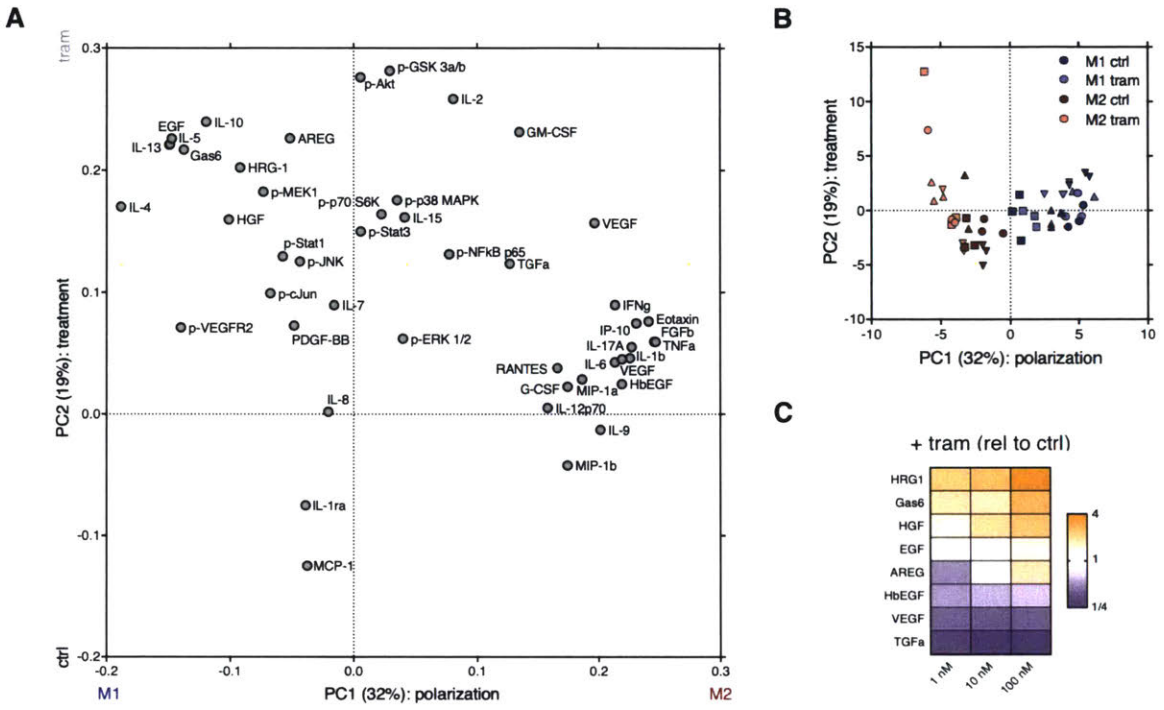

Figure 3-8: MEKi-induced changes in primary monocyte-derived macrophages are reproducible across donors and in monocyte cell line-derived macrophages.

(A,B) Loadings and scores plot generated from PCA of data from Fig. 3-7. Different shapes in (B) represent macrophages differentiated from monocytes isolated from different healthy female donors. (C) Heat map depicting supernatant levels of growth factors (rows) produced by M2-polarized U937-derived macrophages 24 hr following trametinib treatment (varying concentrations in columns), as measured by Luminex.

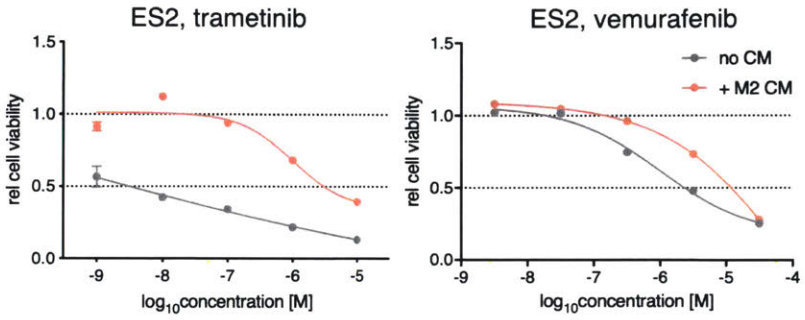

Figure 3-8: Macrophage-conditioned media protects against MAPKi-induced tumor cell killing.

Cytotoxicity curves of ES2 cells treated with trametinib or vemurafenib for 72 hr in the presence or absence of M2-polarized U937-derived macrophage conditioned media. Cell viability was measured with the PrestoBlue assay.

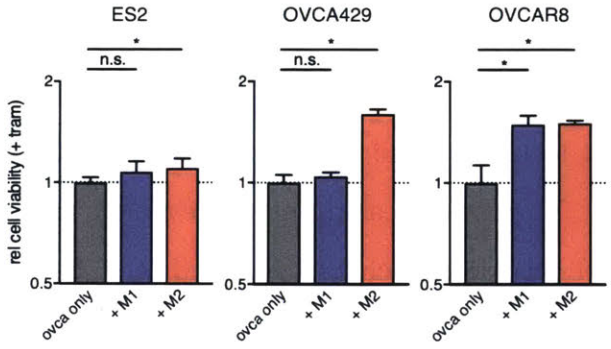

Figure 3-9: Transwell co-culture with macrophages protects against trametinib cytotoxicity.

Three cancer cell lines were treated for 48 hr with trametinib and cultured either alone or in transwell co-culture with M1 or M2 primary monocyte-derived macrophages. Cell viability (amount of $PI^-/Annexin\ V^-$ ovarian cancer cells) was measured by flow cytometry, then normalized to the vehicle-treated control of each culture condition ($^*p < 0.05$, two-tailed ratio t-test).

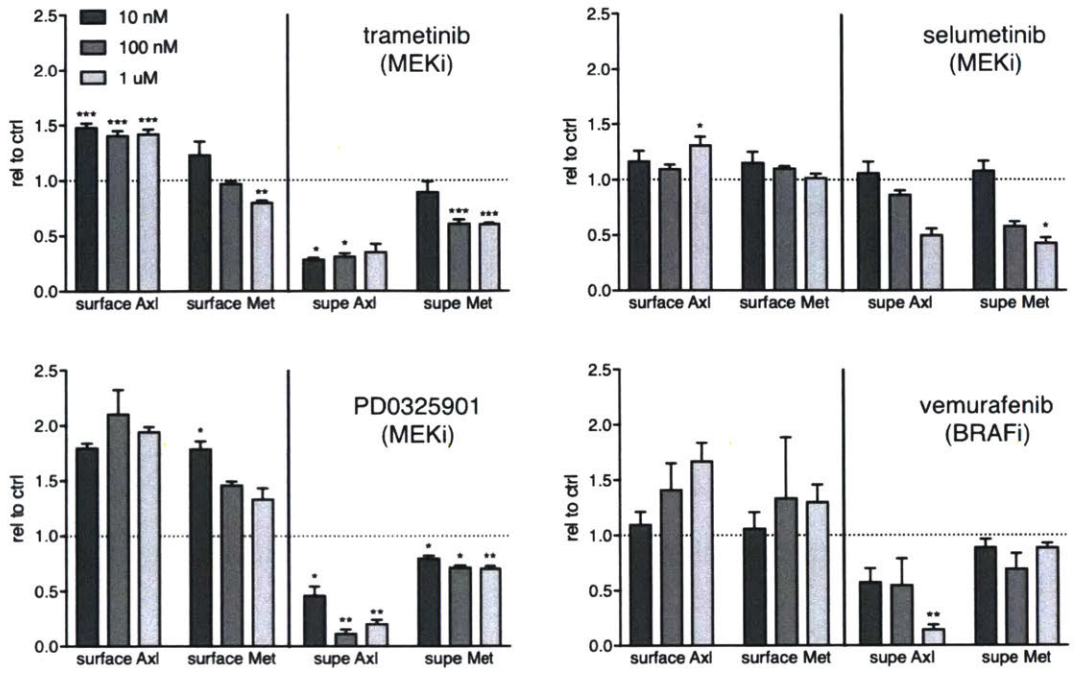

Figure 3-10: MAPKi upregulates surface AXL and MET expression.

ES2 cells' surface (flow cytometry) and supernatant (Luminex) levels of AXL and MET, following 24 hr treatment with varying concentrations of MAPKi (*$p < 0.05$, **$p < 0.01$, two-tailed t-test compared to untreated control).

We next sought to understand how trametinib might affect other aspects of macrophage signaling. Luminex measurements revealed that MEKi upregulated levels of M2-associated cytokines such as IL-13 and IL-4, as well as growth factors such as HGF and Gas6, especially in already M2-polarized macrophages (Fig. 3-7). While univariate analysis of changes in intracellular kinase signaling was not conclusive, multivariate principal components analysis (PCA) demonstrated that phospho-MEK1, -cJun, and -JNK signaling were highly covaried with the upregulated M2-associated signals (Fig. 3-8A). These results were not influenced by donor-to-donor variability and were reproducible in M2-polarized macrophages derived from U937 cells (Fig. 3-8B,C).

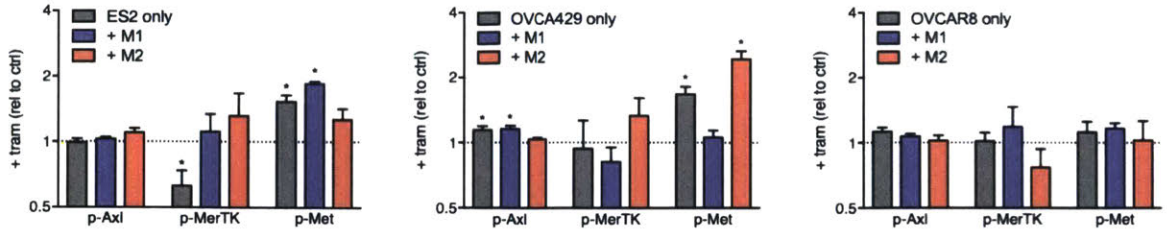

Figure 3-11: Macrophage co-culture alters MEKi-induced RTK activity.

Ovarian cancer cell levels of phospho-AXL, MERTK, MET following 48 hr trametinib treatment and transwell co-culture with or without primary monocyte-derived macrophages (*$p < 0.05$, two-tailed t-test compared to untreated control of own culture condition).

3.2.4 Macrophages protect against trametinib cytotoxicity by amplifying tumor cell RTK and downstream JNK signaling

To assess the influence of the aforementioned macrophage signaling changes on tumor cell phenotype, we measured cell killing caused by MAPKi in the presence or absence of M2-polarized macrophage-conditioned media (Fig. 3-8). Conditioned media protected ES2 cells from BRAFi (vemurafenib IC50 = 686 nM vs. 6 μM, for roughly 10-fold increase) and especially MEKi (trametinib IC50 = 9 nM vs. 1 μM, for roughly 100-fold increase). Similarly, transwell co-culture with M2-polarized macrophages protected the ES2, OVCA429, and OVCAR8 cell lines against trametinib cytotoxicity, while co-culture with M1-polarized macrophages produced a significant effect only in the OVCAR8 line (Fig. 3-9).

Because our ligand-receptor interaction analysis (Fig. 2-4,6) and in vitro macrophage measurements (Fig. 3-7) highlighted the possible importance of Gas6 and HGF signaling in response to MEKi, we wanted to assess their potential impact on tumor cell RTK signaling. Flow cytometric and Luminex measurements of ES2 cells showed that various MAPKi upregulated surface AXL and MET expression,

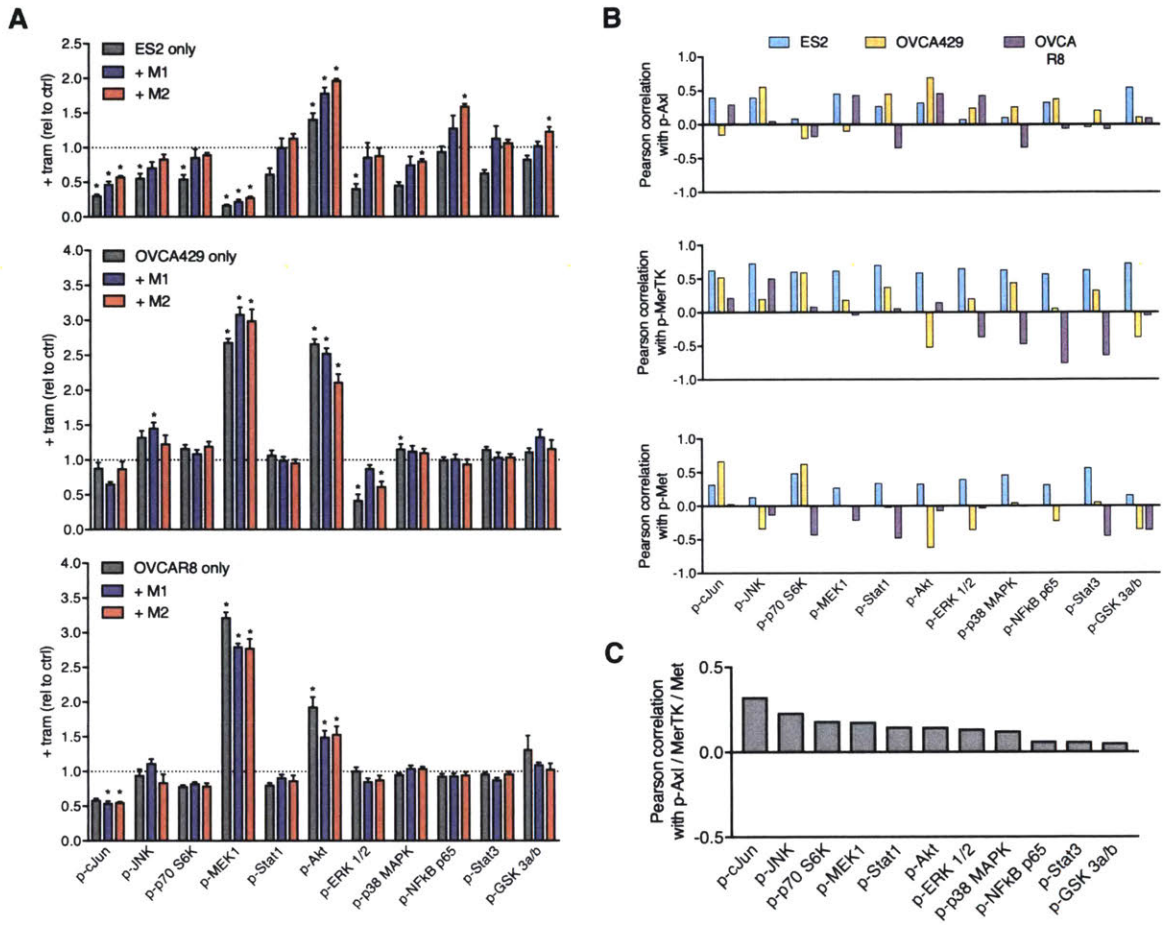

Figure 3-12: JNK/c-Jun activity correlates with bypass RTK signaling.

(A) Ovarian cancer cell levels of active intracellular kinases following 48 hr trametinib treatment and transwell co-culture with or without primary monocyte-derived macrophages (*$p < 0.05$, two-tailed t-test compared to untreated control of own culture condition). (B) Pearson correlation of kinase activity with phospho-RTK levels from Fig. 3-11. (C) Pearson correlation values from (B) averaged across cell lines and RTKs.

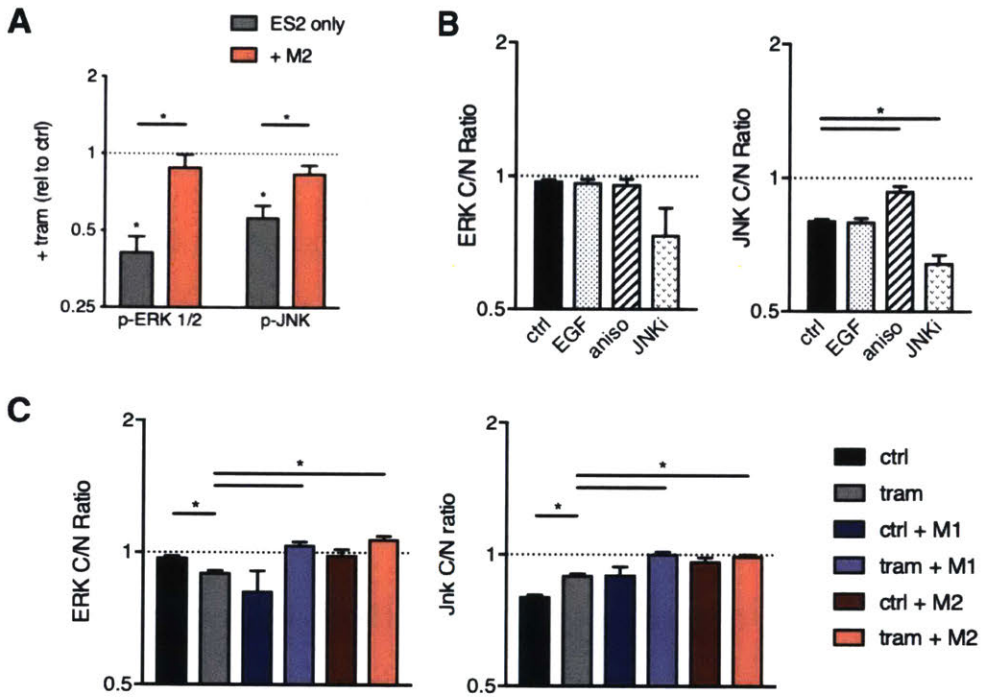

Figure 3-13: Macrophage co-culture attenuates decreases in tumor cell JNK signaling.

(A) Trametinib-induced phospho-ERK and -JNK levels, with or without M2 macrophage transwell co-culture. Partially reproduced from Fig. 3-12A for clarity. (B) In vitro validation of ERK and JNK KTR cytoplasmic/nuclear intensity ratios (C/N ratio). ES2-ECJR cells were treated for 24 hr with EGF = 10 ng/ml exogenous EGF, aniso = 10 μg/ml anisomycin, or JNKi = 10 μM JNK-IN-7. (C) ERK and JNK C/N ratios of ES2-ECJR cells treated with trametinib across various culture conditions. (*$p < 0.05$, two-tailed t-test).

with a concomitant decrease in their shed supernatant levels (Fig. 3-10). This was consistent with previous reports of reduced proteolytic shedding as a post-translational resistance mechanism to MAPKi. [65] This was associated with tumor-intrinsic activation of MET and, to a lesser extent, of AXL across 3 ovarian cancer cell lines (Fig. 3-11). Additionally, transwell co-culture with macrophages altered trametinib-induced tumor cell RTK activity, most notably by enhancing p-MERTK signaling in ES2 and OVCA429 cells.

Multiplex measurements of intracellular kinase signaling demonstrated that JNK/c-Jun activity was most highly correlated with AXL/MERTK/MET signaling across all 3 cell lines' treatment and culture conditions (Fig. 3-12). A closer look indicated that trametinib-induced decreases in ES2 cell p-ERK and p-JNK were attenuated by the presence of M2-polarized macrophages (Fig. 3-13A).

3.2.5 TAMs alter the effect of trametinib on neighboring tumor cell kinase signaling in vivo

To determine whether the aforementioned macrophage-influenced changes in tumor cell signaling states were actually relevant in an in vivo tumor microenvironment, we first transfected ES2 cells with ERK and JNK kinase translocation reporters (KTR). These cells are termed ES2-ECJR (ERK KTR mClover and JNK KTR mRuby). KTRs are fluorescently labeled kinase substrates engineered to convert phosphorylation events to localization changes that can be imaged and subsequently quantified. [89] Specifically, the substrates' nuclear export sequences have been enhanced such that they will shuttle into the cytoplasm if phosphorylated by the kinases whose activities we aim to quantify, leading to greater cytoplasmic versus nuclear fluorescence intensities (C/N ratios) within single cells. The ES2 reporter cells were validated in vitro: the addition of exogenous EGF ligand did not increase the basal ERK C/N ratio as these cells are BRAF-mutant and already constitutively active in MAPK/ERK signaling, while

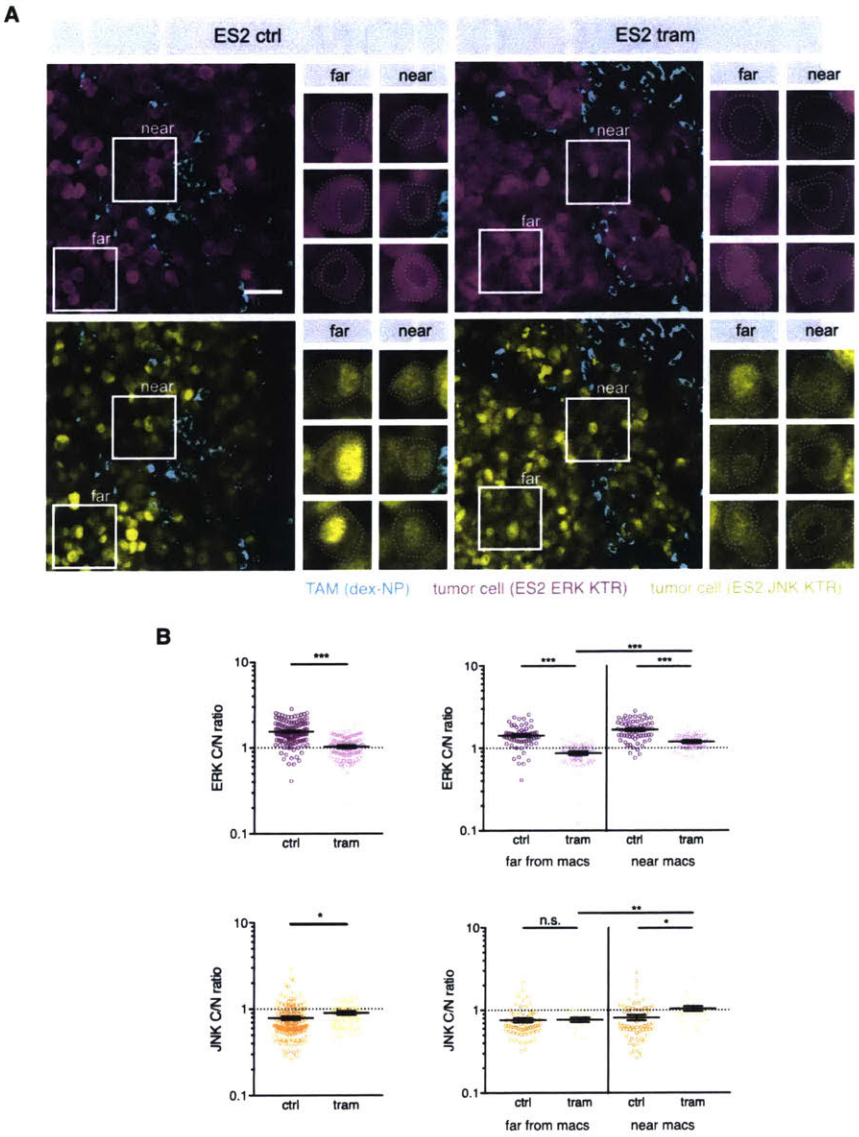

(figure continued on next page)

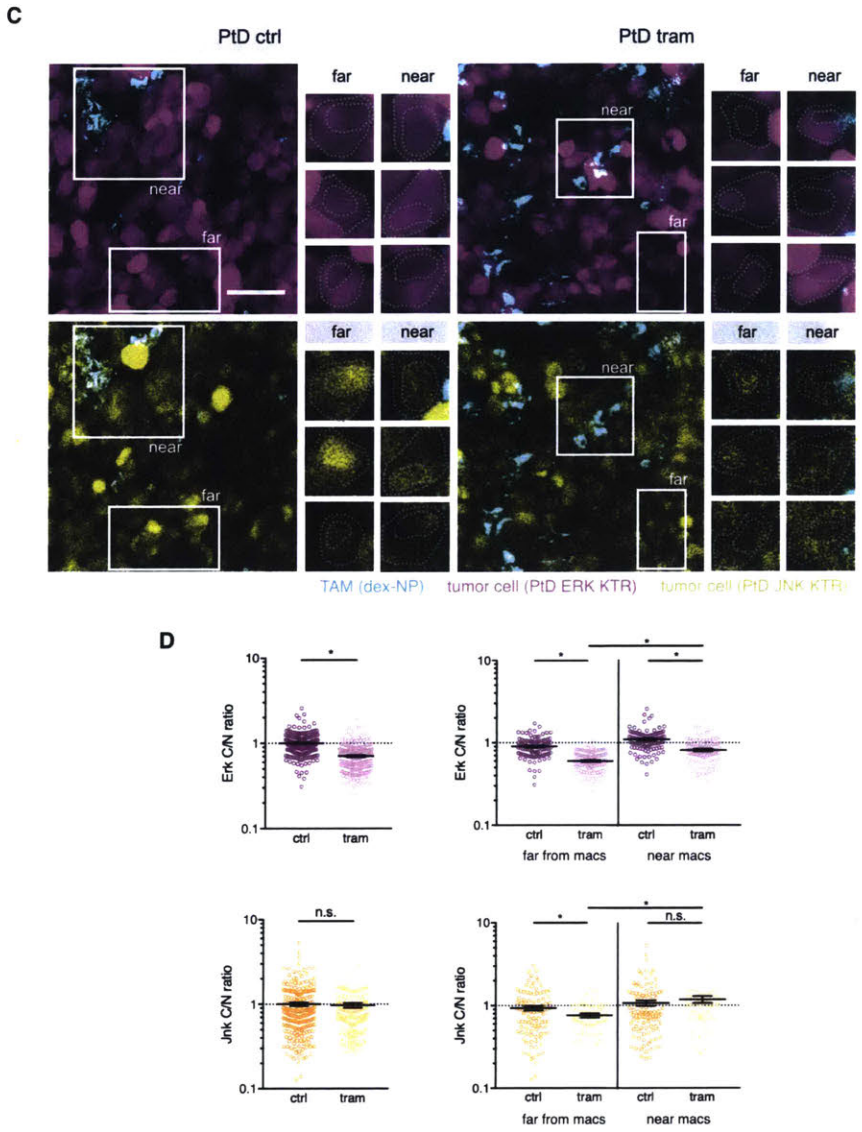

Figure 3-14: Confocal imaging strategy reveals macrophage-influenced JNK signaling.

(A) Representative ex vivo images of fluorescently labeled TAMs and ES2 cells expressing ERK and JNK KTRs. Nu/nu mice with i.p. tumors were treated with oral vehicle or trametinib, then sacrificed 24 hr later to harvest tumors for immediate confocal imaging. (B) Quantification of images including those shown in (A). For each group, a total of 120 cells within 12 tumors from n = 3 mice were quantified. Scale bar: 50 μm. (C,D) Same as (A,B), except using ptD-ECJR cells (*$p < 0.05$, **$p < 0.01$, ***$p < 0.001$, two-tailed t-test).

anisomycin stimulated and the JNK inhibitor JNK-IN-7 lowered the JNK C/N ratio (Fig. 3-13B). Similar to our in vitro Luminex signaling measurements, the presence of macrophages enhanced both ERK and JNK activity in ES2-ECJR cells treated with trametinib (Fig. 3-13C).

To probe single-cell phosphosignaling in vivo, we inoculated nu/nu mice with i.p. ES2-ECJR tumors and, once tumors were established, treated mice with a single dose of oral vehicle or trametinib 24 hr prior to sacrifice. Fluorescent dextran was administered i.v. in order to label macrophages. As expected, ex vivo confocal imaging of harvested i.p. tumors demonstrated widespread tumor cell ERK inhibition with trametinib treatment (Fig. 3-14A,B). Interestingly, compensatory JNK signaling was evident and could be attributed to enhanced activity in ES2-ECJR cells localized near TAMs. The same experiment using ptD cells transfected with the same KTRs (ptD-ECJR) revealed similar results, in that tumor cells near TAMs less frequently experienced MEKi-mediated decreases in JNK signaling (Fig. 3-14C,D).

We next sought to monitor the single-cell activities of p-ERK and p-JNK in real-time following MEKi. To do this, nu/nu mice possessing ES2-ECJR xenograft tumors grown in window chambers were anesthetized and their tumors were imaged on an intravital microscopy platform before and for roughly 1 hr after i.v. trametinib administration. Images of single ES2-ECJR cells near TAMs at their final versus initial imaging time points demonstrated that increases in JNK activity were significantly correlated with decreases in ERK activity (Fig. 3-15A,B,E). Activation of JNK was therefore not due to trametinib inaccessibility within the tumor. While photobleaching did occur due to repeated laser exposure over a short time frame (Fig. 3-15C,D), quantification of single cells near TAMs in control mice indicated that this did not have an effect on ERK and JNK C/N ratios (Fig. 3-15F).

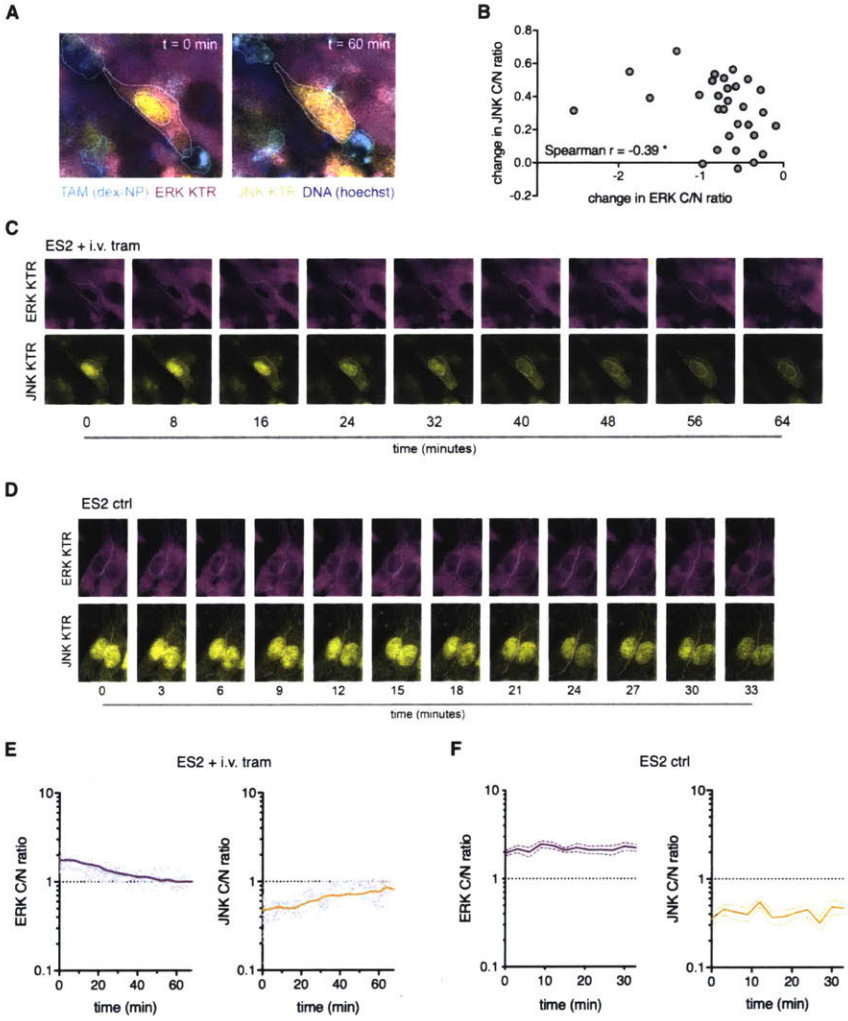

Figure 3-15: Intravital imaging of early signaling kinetics following MEKi.

(A) Representative image of single-cell ERK and JNK signaling before and 60 min after i.v. trametinib administration. Nu/nu mice with ES2-ECJR xenograft tumors grown in dorsal skin-fold window chambers were used. (B) Correlation between changes in ERK and JNK C/N ratios in 20 single cells (*$p < 0.05$). (C) Representative time-lapse images of single-cell kinase activity in mice treated with i.v. trametinib immediately prior to imaging. (D) Same as (C), except with i.v. PBS control injection. (E) Quantification of (C) for 20 single cells, with bolded curves representing the group average. (F) Quantification of (D) for 10 single cells, showing average +/- SEM.

3.3 Discussion

Prior literature has demonstrated the effect of macrophages on therapeutic resistance in other cancers. For example, extensive in vitro studies have demonstrated that vemurafenib (BRAFi) paradoxically activates MAPK signaling in macrophages to produce VEGF, which in turn reactivates MAPK signaling in melanoma cells. [90] Further, macrophage-derived TNF-α was found to confer resistance to MAPKi in BRAF-mutant melanoma by activating anti-apoptotic pathways. [91] Macrophages have also been implicated in ovarian cancer progression, by secreting growth factors such as EGF that promote tumor cell adhesion and spheroid formation during early transcoelomic metastasis. [92] However, the mechanisms through which they might impact therapeutic response, especially in rarer subtypes of ovarian cancer such as those harboring MAPK mutations, are less well-studied.

In our mouse model of intraperitoneally disseminated BRAF-mutant ovarian cancer, we first found that MAPKi directly affects the tumor immune microenvironment by increasing the number of infiltrating TAMs. While enhanced TAM recruitment is likely due to other factors as well, oral administration of maraviroc, an antagonist of the chemokine receptor CCR5, was able to attenuate trametinib-induced TAM influx. Previous studies have shown that the CCL5/CCR5 signaling axis promotes breast cancer progression by not only enhancing monocyte migration into tumor sites, but also enhancing their expression of extracellular matrix-degrading proteases. [93] More recent studies in ovarian and metastatic colorectal cancers have also shown that CCR5 inhibition can reshape macrophage composition and polarization within tumors. [94,95] A phase I trial of maraviroc in patients with chemotherapy-refractory metastatic colorectal cancer achieved partial responses without significant side effects (NCT01736813), indicating the possibility of further exploring the re-purposing of this previously approved HIV drug.

Next, we found that while MEKi-induced macrophage influx was evident,

macrophage depletion with either clodronate liposomes or α-CSF1R antibodies did not significantly enhance MEKi efficacy. Possible explanations include the reasoning that the ES2 BRAF-mutant model's inherent sensitivity to MEKi overshadows any dependency on macrophages, and/or that other communication with other cell types also play a significant role in defining therapeutic response.

Despite this, we still wanted to characterize how these MEKi-induced changes in macrophage proportions might be impacting the tumor. Most notably, we found that MEKi appeared to enhance macrophage M2-associated properties via increased CSF1R expression and enhanced efferocytosis of tumor cell apoptotic bodies. These were accompanied by slight increases in AXL and MERTK expression and activity in M2-polarized macrophages culture in vitro. This corroborates studies performed in other contexts, such as LPS-induced lung injury, where MEKi has been shown to promote macrophage reparative properties via enhanced expression of M2-associated genes and proteins, as well as increased in vivo efferocytosis of apoptotic neutrophils. [96] This is especially interesting in light of the recent failure of IMblaze370, which evaluated MEKi in combination with an anti-PD-L1 antibody in the metastatic colorectal cancer setting. [72] Despite reports of MEKi's ability to activate the anti-tumoral functions of the adaptive immune system, [71] our results suggest that MEKi can also make the tumor microenvironment more immunosuppressive via direct effects on macrophages. Understanding the relative contributions of T cells, macrophages, and likely other cell types will be important for assessing whether it is worthwhile to clinically test MEKi combined with immune checkpoint blockade in other cancer types.

Importantly, MEKi also significantly increased macrophage production of growth factors with the potential to communicate in a paracrine fashion with nearby tumor cell RTKs. These changes in cell-cell communication correlated with protection of ovarian cancer cells against MEKi-induced cytotoxicity, as well as amplification of their RTK and downstream JNK signaling. Given that JNK

signaling is highly context-dependent and that other groups have demonstrated a role for its activation in resistance to chemotherapeutics and targeted therapies including MAPKi, this finding is not necessarily surprising. [97–100]

Overall, we show that multiple bypass pathways operate in parallel and directly measure their downstream effectors (ERK and JNK) in real-time within the in vivo tumor microenvironment. In our intravital imaging experiments using trametinib, decreases in ERK activity were significantly correlated with increases in JNK activity, demonstrating that enhanced JNK signaling was not due to unsuccessful drug delivery to the tumor. However, while trametinib is known for its long half-life enabling sustained target activity, [101] other drugs may have less favorable pharmacokinetic properties, and this may need to be considered if applying in vivo monitoring of single-cell kinase activities towards answering other biological questions.

3.4 Materials and methods

Cell culture. ES2 and U937 cells were obtained from ATCC; ptD and OVCA429 cells were kindly provided by Dr. Ralph Weissleder (Massachusetts General Hospital); and OVCAR8 cells were kindly provided by Dr. Sangeeta Bhatia (Massachusetts Institute of Technology). All cells were grown according to vendor guidelines. Where relevant, cells were then seeded into tissue culture plates such that they were ~80% confluent by the time of experiment endpoint. In conditions were cells were treated with trametinib (Selleck Chem), a 100 nM dose was used unless otherwise specified.

Monocyte isolation from healthy female donors. Peripheral blood mononuclear cells (PBMCs) were isolated from peripheral blood leukapheresis samples from healthy female donors (STEMCELL Technologies) via density gradient centrifugation (Lymphoprep, STEMCELL Technologies). PBMCs were washed 2x with 2% heat-

inactivated FBS and 1 mM EDTA in PBS to remove contaminating platelets, then frozen down in cryopreservation medium (90% heat-inactivated FBS, 10% DMSO) until further use. Immediately prior to differentiation into macrophages, PBMCs were thawed for monocyte isolation via immunomagnetic negative selection (EasySep human monocyte isolation kit, STEMCELL Technologies).

Macrophage differentiation. For monocytes isolated from healthy donors, monocytes were plated at a density of $2*10^5$ cells/ml and 50 ng/ml GM-CSF was added for M1 or 50 ng/ml M-CSF for M2 pre-differentiation. On day 4, an additional 50% of the same cytokine-containing media was added. On day 7, pre-differentiation media was removed and replaced with activation media containing 20 ng/ml IFN-γ + 50 ng/ml LPS (lipopolysaccharides, Sigma) for M1-, or 20 ng/ml IL-4 for M2-polarized macrophages. 24 hr later, macrophages were detached with ice-cold 10 mM EDTA in PBS for seeding into experimental culture plates. For differentiation of U937 monocytes into macrophages, a similar protocol was performed, except monocytes were plated at a density of $5*10^5$ cells/ml and incubated with media containing 50 ng/ml PMA (phorbol 12-myristate 13-acetate, Sigma) for 1 day in place of the 6-day pre-differentiation step. The growth factors and cytokines used here were purchased from Peprotech unless otherwise stated.

Conditioned media and co-culture assays. Conditioned media was generated by treated macrophages with varying concentrations of trametinib where indicated, concentrated using Amicon spin filters (3 kDa, EMD Millipore) to remove free drug, then resuspended in fresh media along with the appropriate concentration of fresh drug. Cell viability was measured via PrestoBlue (Invitrogen) following a 72 hr incubation period. For transwell co-culture assays, we used 24-well plates containing polycarbonate transwell inserts with 0.4 μm pores (Corning). $5*10^4$ macrophages were seeded in the inner insert, while $1*10^5$ or $5*10^4$ ovarian cancer cells were seeded in the well bottom for endpoint signaling measurements (24 hr

incubation) or phenotypic measurements (48 hr incubation), respectively.

Luminex assays for cell culture supernatants. The Bio-Plex Pro human cytokine 27-plex assay (Bio-Rad) was used to measure levels of various cytokines, while individually coupled magnetic beads were used to detect growth factors. To generate our own immunoassays, we used capture and detection antibodies against human HRG1, GAS6, HGF, EGF, AREG, HB-EGF, VEGF, and TGF-α purchased as DuoSets from R&D Systems. For antibody-bead coupling, Bio-Plex Pro magnetic COOH beads (Bio-Rad) were activated with EDC (N-(3-dimethylaminopropyl)-N'-ethylcarbodiimide, Sigma) and sulfo-NHS (N-hydroxysulfosuccinide, Pierce) in 100 mM phosphate buffer (pH 6.3) for 20 min shaking at room temperature, then incubated with 0.1 mg/ml capture antibody in 50 mM HEPES buffer (pH 7.4) overnight shaking at 4C. The following day, beads were washed 3x in 1% BSA in PBS, then stored at 4C. Immunoassays were adapted to a 384-well plate format, performed on 1x or 1/10x dilutions of clarified supernatants according to manufacturers' protocols, and read on a FLEXMAP 3D system (Luminex Corp). For each analyte, 5-parameter logistic regression was used to fit standard curves for absolute quantification. Measured levels of analytes were normalized based on the micro BCA protein assay (Pierce). Due to the relatively large number of analytes measured within each assay, the Benjamini-Hochberg procedure was used to correct for multiple comparisons between treatment conditions.

Luminex assays for cell culture lysates. A custom Bio-Plex phosphoprotein panel was used to measure levels of intracellular kinases and consisted of immunoassays detecting phosphorylated versions of cJun, JNK, p70 S6K, MEK1, Stat1, Akt, ERK1/2, p38 MAPK, NFkB p65, Stat3, and GSK 3a/b. R&D DuoSets against human AXL, MERTK, MET, and CSF1R were used to generate immunoassays

against these RTKs. Bio-Plex cell lysis buffer (Bio-Rad) was used to lyse cells for intracellular kinase measurements, while NP40 cell buffer (20 mM Tris-HCl, 150 mM NaCl, 2 mM EDTA, 1% NP40, 10% glycerol, pH 7.4) was used for RTK measurements. In both cases, immunoassays were performed on clarified lysates diluted 2-fold in assay buffer consisting of 1% BSA in PBS.

Flow cytometry. Ovarian cancer cells were gently detached with Versene (Gibco) prior to staining. For phenotypic measurements, cells were stained with Annexin V FITC and propidium iodide (Dead Cell Apoptosis Kit, Invitrogen). For RTK expression measurements, cells were stained with anti-human AXL-AF700 (clone #108724, R&D Systems) and anti-human MET-PE (clone #95106, R&D Systems), as well as a LIVE/DEAD fixable stain (Invitrogen) to gate out dead cells. After washing and resuspension, samples were run on an Accuri C6 flow cytometer (BD Biosciences), and data were analyzed using FlowJo software (FlowJo LLC).

Efferocytosis assay. We generated fluorescent apoptotic bodies by treating CellTracker Deep Red-labeled (Invitrogen) ES2 cells with 10 mM trametinib for 48 hr. Supernatants were harvested and apoptotic bodies were purified by sequential centrifugation for 10 min at 300 g, then 10 min at 2000 g. Apoptotic bodies were resuspended in fresh media and incubated with pre-treated M2-polarized primary monocyte- or U937-derived macrophages (100 nM trametinib or DMSO control, 24 hr) for 4 hr. Macrophages were detached with 10 mM EDTA, stained with propidium iodide, then run through an Accuri C6 flow cytometer to assess uptake of apoptotic bodies.

Generation and validation of cell lines expressing KTRs. ES2-ECJR or ptD-ECJR cell lines were established by lentiviral transfection with the ERK KTR mClover and JNK KTR mRuby2 constructs (Addgene plasmids #59150 and #59154). [89] To validate these reporter cell lines in vitro, we seeded 40,000 cells/well into a 24-

well μ-plate (Ibidi), then treated the following day with EGF (Peprotech), anisomycin (Sigma), or JNK-IN-7 (MedChemExpress). After a 24 hr incubation period, cells were fixed with warm 4% PFA in PBS for 15 min, stained with 1 μg/ml Hoechst 33342 (Invitrogen) for 10 min, and finally imaged with a Leica DMI 6000 microscope and Oasis Surveyor software. CellProfiler (Broad) was used to process images by segmenting single cells into their cytoplasmic versus nuclear compartments, and then quantifying the cytoplasmic-to-nuclear intensity ratios of mClover and mRuby2 fluorescence. The results generated from this pipeline confirmed that the cellular localization of these reporters serves as a proxy for kinase activity.

Studies with mouse models of intraperitoneally disseminated ovarian cancer. Experimental models of i.p. disseminated ovarian cancer were established by injecting $5*10^6$ ES2-ECJR or ptD-ECJR cells suspended in 200 μl PBS into the peritoneal cavity of 6-8 weeks old female nu/nu mice (Massachusetts General Hospital Cox 7 Core). All animal research was performed in accordance with guidelines from the Institutional Subcommittee on Research Animal Care. Tumors were allowed to grow for about 2 weeks prior to treatment for imaging studies and for about 1 week prior to treatment for efficacy studies. Mice were semi-randomized into groups depending on body weight. Both mouse models develop ascites upon tumor progression, which is characteristic of human disease. Where indicated, mice were treated with 0.3 mg/kg trametinib (1% DMSO, 0.5% methylcellulose, 0.2% Tween80 in water; Selleck Chem) and/or 30 mg/kg maraviroc (5% DMSO, 0.5% 0.1N HCl in water; Selleck Chem) via oral gavage. [102,103] For studies involving macrophage depletion via clodronate liposomes, 150 μl 5 mg/ml clodronate or control liposomes (Liposoma BV) were injected i.p. on day 1 of the study, followed by 50 μl every 3 days thereafter. For studies involving macrophage depletion via α-CSF1R antibodies, 200 μg InVivoMAb anti-mouse CSF1R (clone AFS98,

BioXCell) or rat IgG2a isotype control (clone 2A3, BioXCell) were injected i.p. beginning on day 1 of the study, followed by 2-3x a week thereafter.

Preparation of fluorescent macrophage labels. Carboxymethylated poly-glucose nanoparticles (macrin-NPs) were synthesized as in [104]. For fluorophore conjugation, 20 mg macrin-NP (containing 7.6 μmol amines) was dissolved in $NaHCO_3$ buffer (2 ml, 0.1 M, pH 8.5) and Pacific Blue-NHS ester (0.27 μmol, Invitrogen) was added. The reaction mixture was shaken for 3 hr at room temperature on a thermomixer (900 rpm), then concentrated using Amicon spin filters (10 kDa, EMD Millipore). To succinylate all remaining amines, Pacific Blue-labeled macrin-NPs were treated with triethylamine (2 μl) and succinic anhydride (100 ul, 750 mM in DMSO) in MES buffer (200 ul, 50 mM, pH 6.0). Following overnight shaking (900 rpm) at room temperature, the mixture was then purified using a PD-10 column (GE Healthcare) with diH_2O as the eluent. Fractions containing labeled, succinylated macrin-NPs (macrin) were concentrated using 10 kDa MWCO Amicon spin filters, then lyophilized for resuspension in PBS. Similarly, 500-kDa amino-dextran (Thermo) was labeled with Pacific Blue-NHS ester, then purified using 30 kDa Amicon spin filters. The amount of macrophage label (corresponding to 5 nmol dye) to be injected intravenously was determined via NanoDrop (ThermoFisher) measurements.

Ex vivo imaging. Fluorescent macrin or dextran was administered intravenously, and 24 hr later, mice were euthanized and tumor-bearing organs (ovaries, uterine fat pads, liver, omentum) were harvested for immediate imaging on a FluoView FV1000MPE confocal imaging system (Olympus America). Numbers of fluorescently labeled macrophages and ERK KTR-expressing tumor cells were quantified using maximum projections across an equal number of 20x-3z z-stack slices in ImageJ (NIH). Intensity measurements of ERK and JNK KTRs from

images acquired with the same acquisition settings were background-corrected prior to calculating C/N ratios for single tumor cells.

Intravital imaging of xenograft tumors in window chambers. 2 million ES2-ECJR cells in 50 μl PBS were injected under the fascia following implantation of titanium dorsal skin-fold window chambers (APJ Trading) in nu/nu mice. Xenograft tumors were allowed to grow for approximately 2 weeks prior to treatment administration and imaging on a FluoView FV1000MPE confocal imaging system.

4 Translational strategy against reciprocal bypass signaling

4.1 Introduction

The previous chapter demonstrated that multiple compensatory signaling pathways operate in parallel to mediate MAPKi resistance. Upon trametinib administration, ovarian tumor cells upregulated the chemokine CCL5, leading to enhanced recruitment of macrophages. In turn, these macrophages promoted an immunosuppressive environment via increased efferocytosis of tumor cell apoptotic debris and, importantly, via production of locally supplied growth factors which further amplified tumor-autonomous RTK pathways and downstream JNK signaling.

In this chapter, we aim to develop a combination therapy to target this reciprocal TAM-tumor crosstalk for overcoming resistance. We hope to rationally identify pharmacological perturbations that are synergistic with MEKi based on the systems-level signaling measurements obtained in Chapter 3, evaluate their effects on intercellular communication, and develop a strategy for effective in vivo delivery.

4.2 Results

4.2.1 Multikinase inhibition is synergistic with trametinib, especially in the presence of macrophage-conditioned media

To understand how our systems-level analysis of TAM-tumor crosstalk might lead to a viable therapeutic strategy, we tested whether macrophage-conditioned media might sensitize ES2 cells to RTK bypass inhibition. The addition of an AXL Fc chimera or a HGF neutralizing antibody significantly enhanced trametinib cytotoxicity in the presence of M2-polarized macrophage-conditioned media, while neither had an effect in the presence of control growth media (Fig. 4-1). In the presence of M1-polarized macrophage-conditioned media, only the HGF neutralizing antibody was sensitizing, corroborating previous observations that MEKi caused M1-polarized macrophages to upregulate growth factor production to a lesser extent than M2-polarized macrophages.

We next treated ES2 cells with combinations of MAPKi and RTKi, and then fit the resulting cell viability measurements to a model of Loewe additivity. This model takes a given cell viability surface as input in order to fit an interaction parameter α, which reflects the degree of synergy (more-than-additive effects) between two drugs (Fig. 4-2A). Out of all tested combinations of MAPKi with AXLi, METi, or multikinase inhibition (MKi), co-treatment with trametinib and foretinib yielded the highest level of synergy. This synergy was significantly enhanced with the addition of exogenous Gas6 (but not HGF or EGF), and especially in the presence of M2 macrophage-conditioned media (Fig. 4-2B,C,E). Synergistic interactions were ablated with an AXL Fc chimera, suggesting that the GAS6-AXL/MERTK signaling axis contributes to macrophage-mediated MEKi resistance.

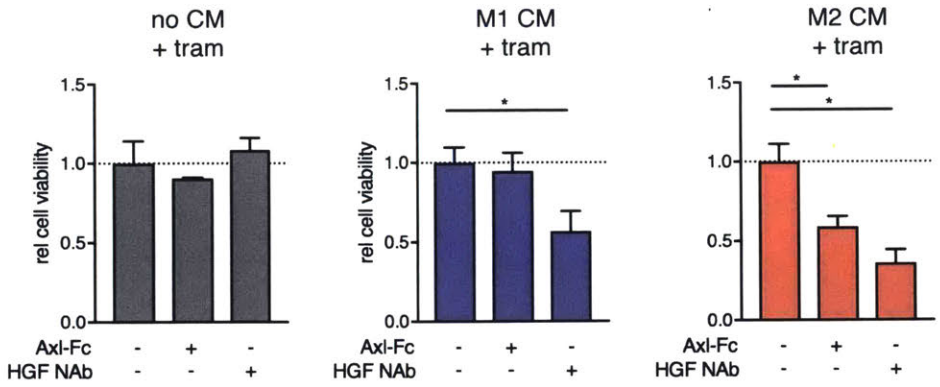

Figure 4-1: Macrophage-conditioned media sensitizes tumor cells to RTK bypass inhibition.

PrestoBlue measurements of ES2 cells treated with trametinib +/- M1 or M2 macrophage-conditioned media +/- inhibitors of growth factor-RTK signaling. Axl-Fc = Axl Fc chimera, HGF Nab = HGF neutralizing antibody (*p < 0.05, two-tailed t-test).

Foretinib is a MKi that binds tightly to AXL, MERTK, MET, and CSF1R, among others. Co-treatment with foretinib significantly reduced trametinib-induced compensatory AXL and MET activity in ES2 mono-cultures (Fig. 4-3A), as well as CSF1R expression in M1- and M2-polarized macrophages (Fig. 4-3B,C). Interestingly, MERTK expression and activity in M2-polarized macrophages was also substantially decreased with the addition of foretinib, suggesting potential immunomodulatory effects.

4.2.2 Nano-foretinib preferentially targets TAMs

We next sought to determine the optimal delivery method for foretinib and considered a recently published CRISPR screen aimed at identifying regulators of phagocytosis. [105] Gene set enrichment analysis (GSEA) demonstrated that knockout of MAPK/ERK signaling enhanced phagocytosis of negatively charged 300 nm-diameter carboxy-coated beads (Fig. 4-4), suggesting that nanoparticle delivery might be a viable strategy for therapeutically targeting TAM-tumor crosstalk that has been upregulated as a result of MEKi.

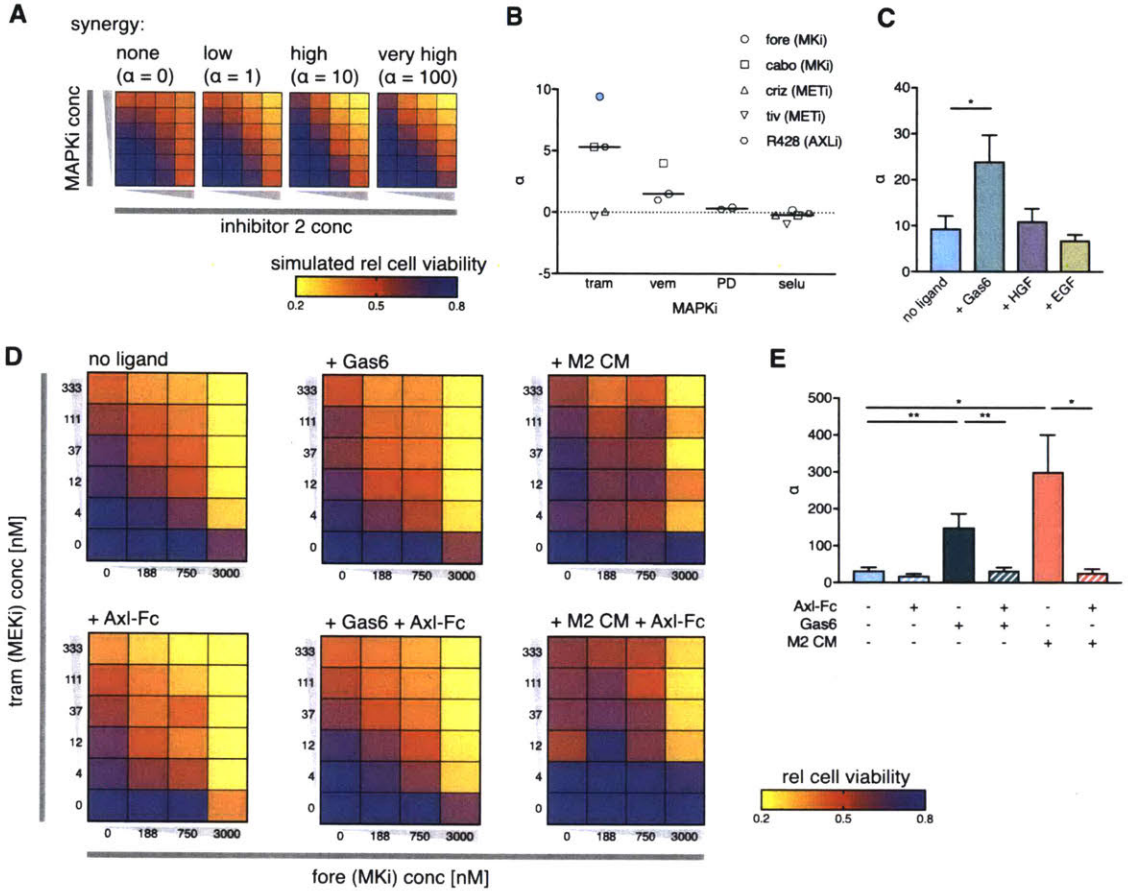

Figure 4-2: Multikinase inhibition is synergistic with trametinib, especially in the presence of macrophage-conditioned media.

(A) Simulated cell viability surfaces corresponding to varying levels of Loewe synergy, as indicated by the interaction term α. (B) Combinations of MAPKi and RTKi (different shapes) were empirically screened for synergy in ES2 cells via the PrestoBlue assay. Fore = foretinib, cabo = cabozantinib, criz = crizotinib, tiv = tivantinib. Most synergistic trametinib + foretinib combination is indicated in light blue. (C) α-value of trametinib + foretinib combination with the addition of 100 ng/ml exogenous ligands. (D) Cell viability surfaces for the same combination with the addition of M2-polarized, U937-derived macrophage-conditioned media and/or various exogenous factors (400 ng/ml Gas6, 1 μg/ml Axl-Fc). (E) Fractional survival data from (D) was fit to a model of Loewe synergy (*$p < 0.05$, **$p < 0.01$, two-tailed t-test).

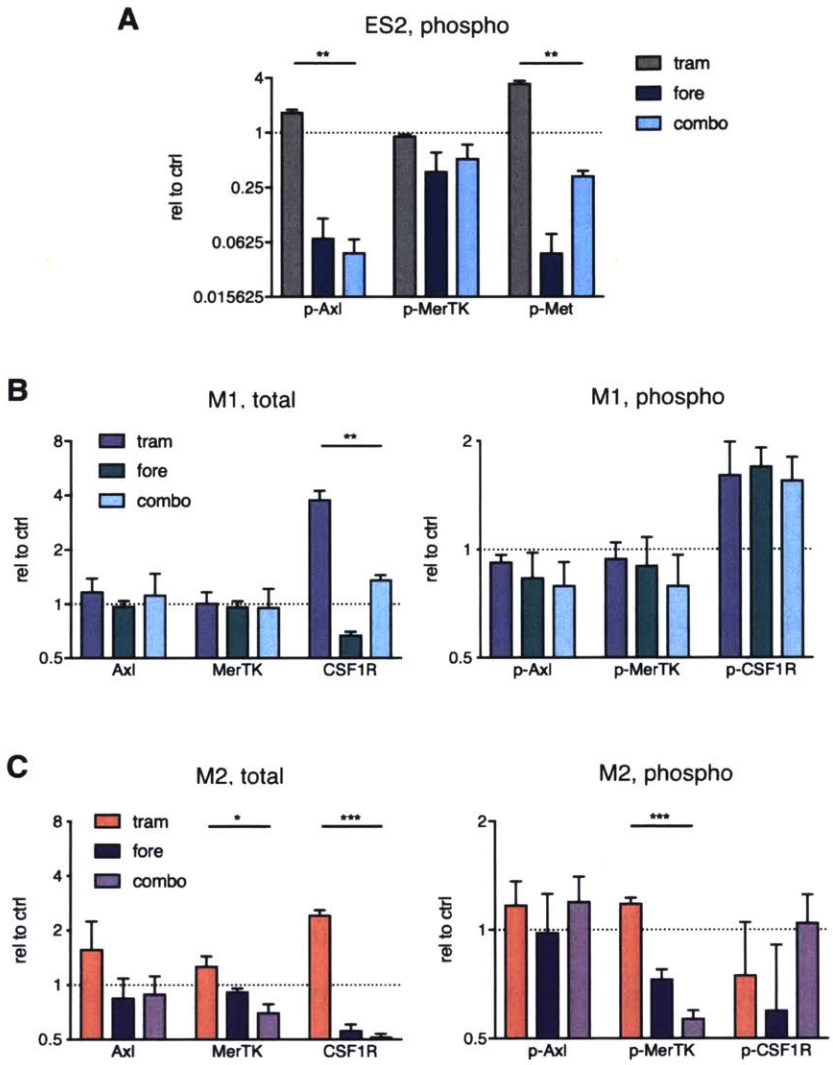

Figure 4-3: Combination therapy yields RTK signaling changes in both tumor cells and macrophages.

(A) ES2 levels of select p-RTKs following 24 hr treatment with trametinib, foretinib, or the combination, as measured by Luminex. (B) M1-polarized and (C) M2-polarized macrophage levels of select total and p-RTKs following the same treatments as in (A) (*p <0.05, **p <0.01, *** p <0.001, two-tailed t-test).

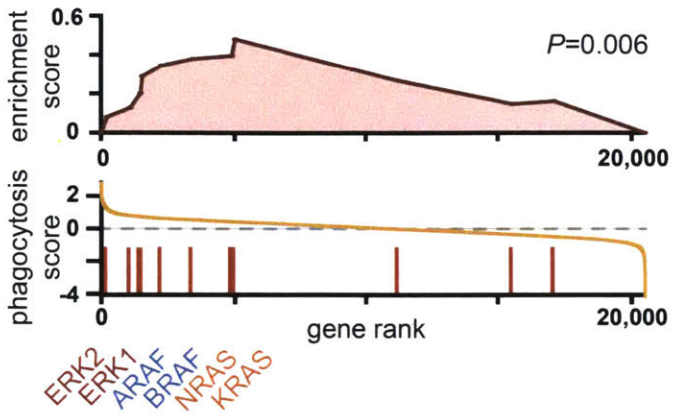

Figure 4-4: CRISPR disruption of MAPK/ERK signaling enhances phagocytosis in U937 cells.

GSEA evaluating enrichment of MAPK/ERK pathway members in published CRISPR screen for regulators of phagocytosis.

We optimized encapsulation of the MKi foretinib in ~60 nm 5 PEG-PCL : 1 PLGA nanoparticles (Fig. 4-5A), which retained cytotoxicity against ES2 cells (IC50 = 1.8 μM vs. 1.7 μM for foretinib dissolved in DMSO, Fig. 4-5B). When injected i.p., fluorescently labeled nano-foretinib (BODIPY630-nano-foretinib) accumulated in the systemic circulation with a half-life of roughly 60 min and, with a decay half-life of roughly 90 min, was cleared and re-distributed preferentially to i.p. tumors with minimal accumulation in healthy tissue (Fig. 4-5C,D).

Ex vivo confocal imaging demonstrated that fluorescently labeled nano-foretinib co-localized preferentially to TAMs, as opposed to ES2 cells and other host cells (Fig. 4-6A). Moreover, although MAPK/ERK signaling acts as a negative regulator of phagocytosis (Fig. 4-4), the localization fraction of nano-foretinib with TAMs was only slightly increased upon systemic MEKi administration (Fig. 4-6A). This could be due to a number of factors, including but not limited to the fact that MAPK reactivation is known to occur in BRAF wild-type cells such as TAMs. Nevertheless, as shown through fluorescence reflectance imaging, MEKi enhanced

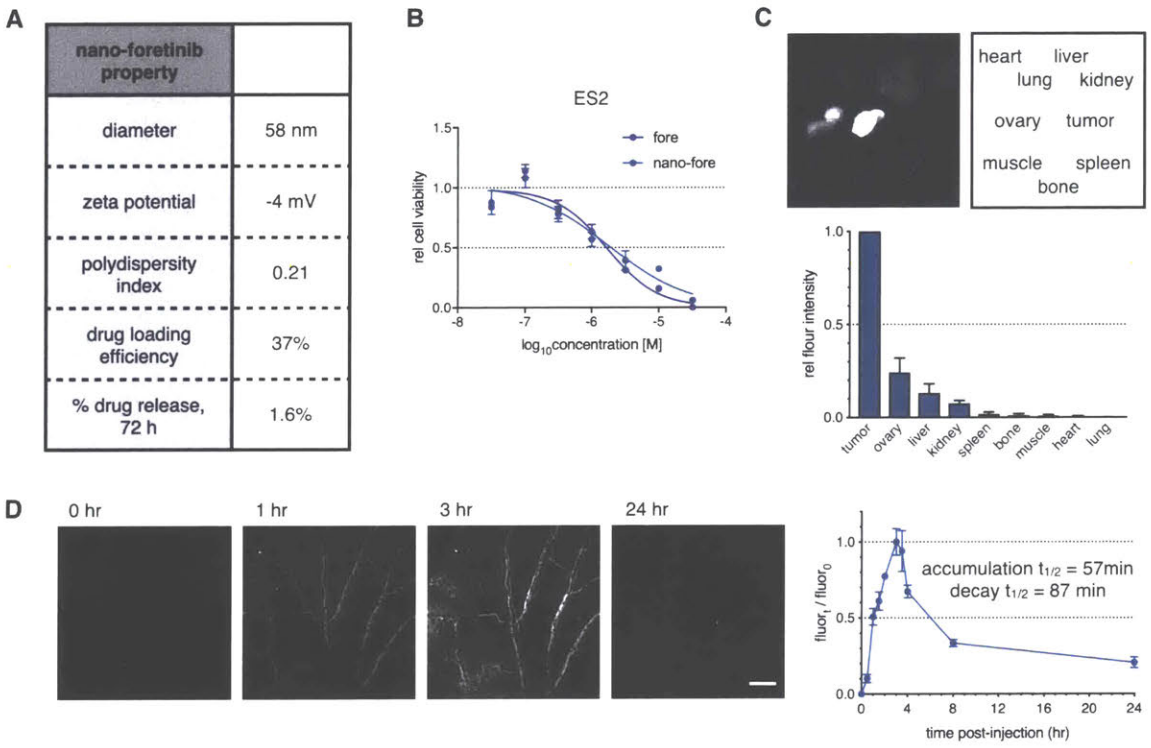

Figure 4-5: Nano-foretinib characterization.

(A) Table listing nano-foretinib properties. (B) Cytotoxicity curves of foretinib vs. nano-foretinib with ES2 cells. (C) Representative fluorescence reflectance image and quantified biodistribution of BODIPY630-nano-foretinib. ES2 i.p. tumors and organs were harvested 24 hr after i.p. injection of nanoparticles into n = 3 nu/nu mice. (D) Confocal images of healthy mouse ear at select time points following i.p. injection of BODIPY630-nano-foretinib at t = 0 hr. Systemic accumulation and decay half-lives were quantified via fluorescence of n = 10 vessels.

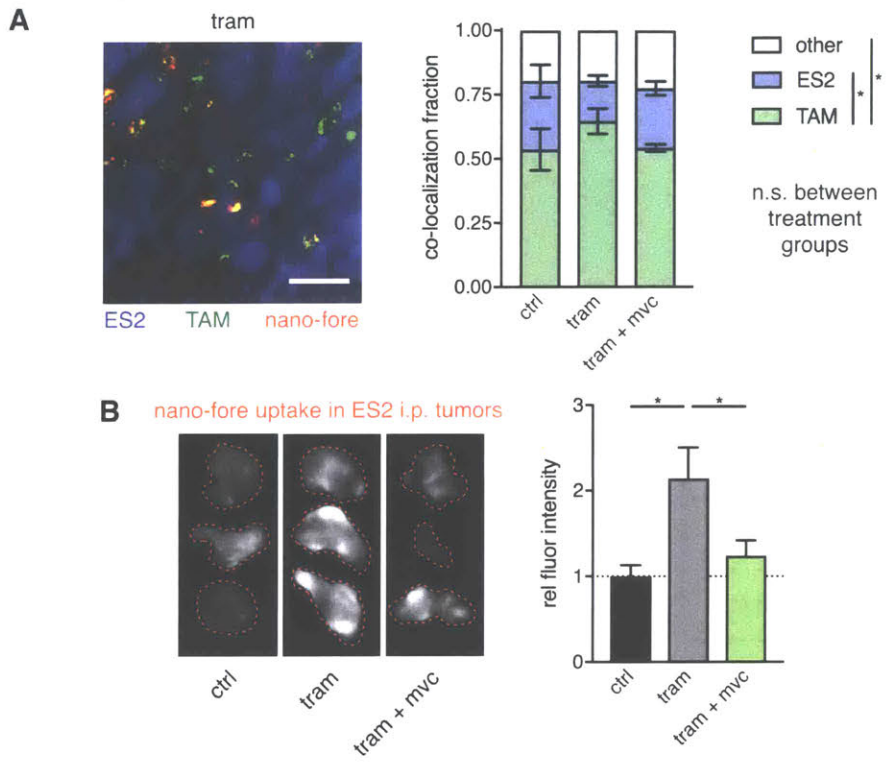

Figure 4-6: Nano-foretinib localizes preferentially to TAMs.

(A) Representative image and quantification of fluorescently labeled ES2 cells, TAMs, and nano-foretinib within i.p. tumors excised 24 hr after i.p. BODIPY630-nano-foretinib injection and 3x daily oral treatments of either vehicle, trametinib, or trametinib + maraviroc. Nano-foretinib was classified as co-localized to TAMs, ES2 cells, or other cells. At least 10 cells were quantified per tumor, with multiple tumors imaged from n = 3 nu/nu mice per group. Scale bar: 50 um. (B) Representative fluorescence reflectance image and quantification of BODIPY630-nano-foretinib uptake in same ES2 i.p. tumors from (A) (*p $<$ 0.05, two-tailed t-test).

nano-foretinib uptake in ES2 i.p. tumors, and this increase was mitigated with the addition of maraviroc. Overall, uptake of these nanoparticles was highly correlated with the extent of macrophage infiltration across the 3 treatment groups (Fig. 3-3), suggesting that nano-foretinib therapeutically exploits MEKi-mediated macrophage recruitment.

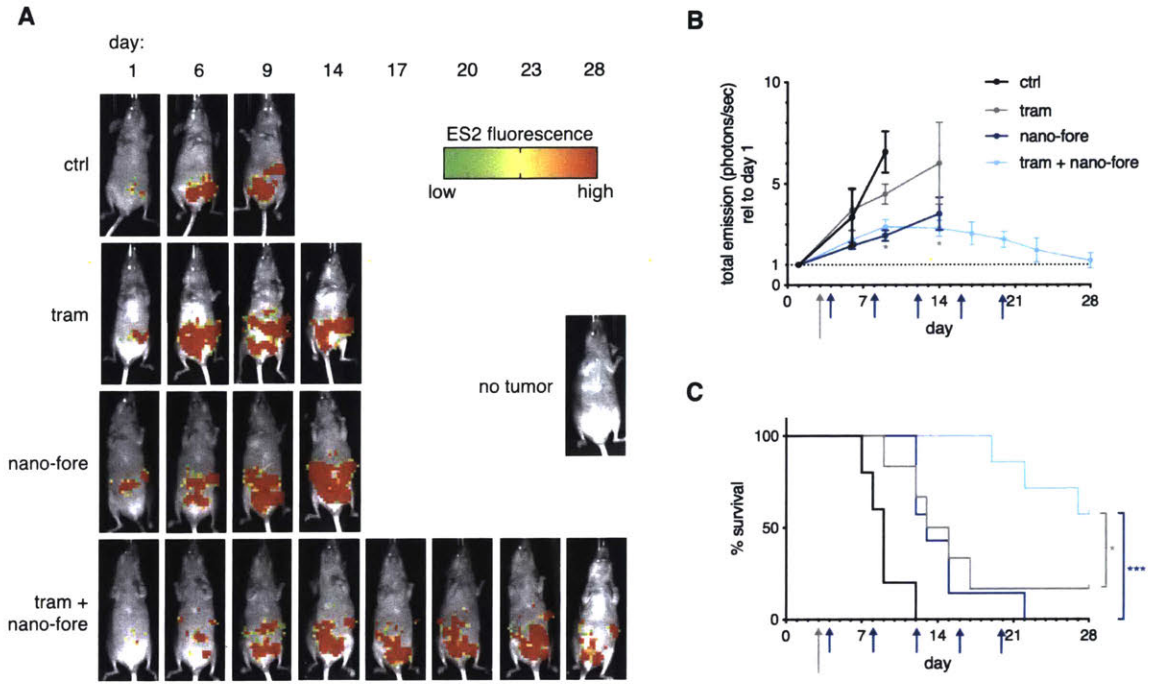

Figure 4-7: Nano-foretinib synergizes with trametinib in vivo.

(A) Representative whole-body fluorescence images of nu/nu mice with ES2 i.p. tumors treated with trametinib, nano-foretinib, or the combination. (B) Quantification of tumor burden. Large gray arrow denotes beginning of daily trametinib administration, while smaller blue arrows denote i.p. nano-foretinib injection time points. $n \geq 5$ mice per group (*$p < 0.05$, two-tailed t-test). (C) Kaplan-Meier survival curves of same mice as in (B). (*$p < 0.05$, ***$p < 0.001$, log-rank test).

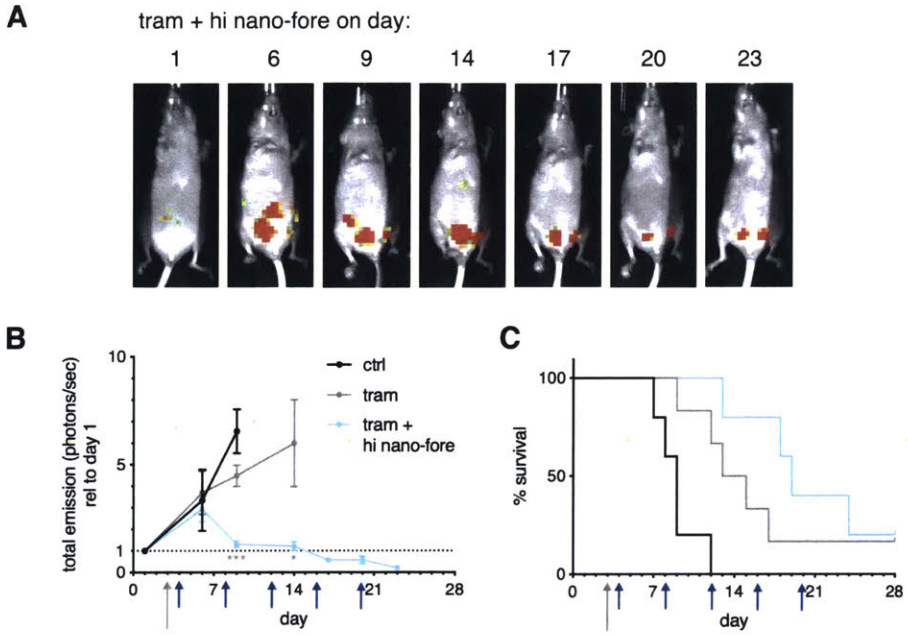

Figure 4-8: High-dose nano-foretinib and trametinib combination causes tumor regression but does not significantly extend survival.

(A) Representative whole-body fluorescence images of nu/nu mice with ES2 i.p. tumors treated with high-dose nano-foretinib and trametinib combination. (B) Quantification of tumor burden. Control and trametinib groups reproduced from Fig. 4-7 for comparison. n $\geq$ 5 mice per group (*p $<$ 0.05, ***p $<$ 0.001, two-tailed t-test). (C) Kaplan-Meier survival curves of same mice as in (B).

4.2.3 Nano-foretinib combines with trametinib to extend survival

In vivo, trametinib and nano-foretinib synergized to significantly reduce tumor burden and extend survival compared to either drug alone (Fig. 4-7). While higher doses of nano-foretinib co-treatment led to complete tumor regression in a highly aggressive mouse model, it did not extend survival, possibly due to systemic toxicity (Fig. 4-8). Combination-treated mice (from Fig. 4-7) sacrificed at their survival endpoints possess less TAMs than their control- or trametinib-treated counterparts (Fig. 4-9A). It remains unclear whether this was due to decreased macrophage recruitment to tumor sites, cytotoxicity against already infiltrated

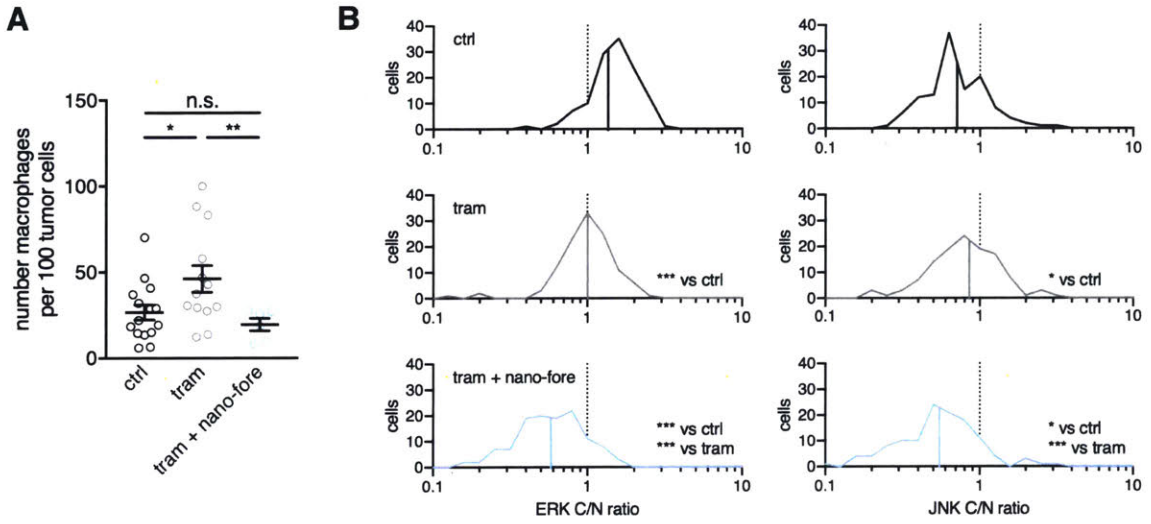

Figure 4-9: Nano-foretinib reduces trametinib-induced macrophage infiltration and compensatory JNK signaling.

Quantification of (A) macrophage infiltration and (B) single-cell ERK and JNK activity in ES2 i.p. tumors excised from nu/nu mice at survival endpoints. (*$p < 0.05$, **$p < 0.01$, ***$p < 0.001$, two-tailed t-test).

TAMs, or both. Regardless, this correlated with further decreases in ERK activity and ablation of compensatory JNK activity (Fig. 4-9B).

4.3 Discussion

Systems biology efforts can bring forth understanding of complex intra- and intercellular signaling networks and therefore shed light on potential tumor cell co-dependencies. With this in mind, we utilized tool compounds targeting key TAM-tumor signaling nodes to demonstrate that neutralization of macrophage-supplied growth factors was sufficient to increase ovarian cancer cell sensitivity to MEKi. To test if there are therapies that can mimic the effects of our in vitro pharmacological perturbations, we evaluated combinations of various MAPKi with

RTKi and assessed their synergy using a model of Loewe additivity. We found that the MEKi trametinib highly synergized with the MKi foretinib, especially in the presence of GAS6 produced by macrophages, and therefore chose to evaluate this combination in a pre-clinical model.

In a mouse model of intraperitoneally disseminated ovarian cancer, relative to monotherapy with trametinib, the combination therapy reduced the amount of TAMs and levels of tumor cell ERK and JNK activity. A recently published screen of kinase inhibitors against human osteosarcoma cells identified foretinib as a potent inducer of immunogenic cancer cell death. [106] Immunogenic cancer cell death is characterized by various changes to tumor cells upon dying that enable cells of the adaptive immune system to generate an anti-tumor response. [107] Examples of such changes include the passive release of HMGB1 – a non-histone-chromatin-binding protein that influences transcription and other nuclear functions – by dying tumor cells, which binds to Toll-like receptor 4 on dendritic cells and initiates an inflammatory response through processing and presentation of tumor-derived antigens. Furthermore, immunogenic cell death is also associated with the translocation of calreticulin from the endoplasmic reticulum lumen to the plasma membrane upon initiation of apoptosis. This mediates the rapid recognition and phagocytosis of tumor cells by dendritic cells, in turn leading to a potent anti-tumor response via cytotoxic T cells. In a separate study, inhibition or gene knockdown of MERTK was shown to impair efferocytosis and reduce proportions of M2-like macrophages in a mouse model of mammary tumor metastasis. [87] Because foretinib binds to MERTK with a K_D of 0.3 nM (based on KINOMEscan data from HMS LINCS: Harvard Medical School Library of Integrated Network-based Cellular Signatures collection) and has been shown here to directly decrease M2-polarized macrophage MERTK expression and activity, we hypothesize that it would have similar immunomodulatory effects.

While we did not directly assess the effects of trametinib and nano-foretinib on macrophage (or other immune cell) polarization and function in vivo, highly

multiplexed approaches would likely be useful for answering these biological questions and understanding how these therapies might be best combined with other promising immunotherapies. This would also require the use of fully immunocompetent, syngeneic mouse models, which do not yet exist for MAPK-mutant ovarian cancer. While the ID8 ovarian cancer model syngeneic to C57BL/6 mice is often used, it serves as a better representation of MAPK wild-type, high grade serous disease. Genetically engineered mouse models that spontaneously form MAPK-driven ovarian tumors are now in development and will hopefully pave the way for fruitful studies to come.

In order to enhance delivery of foretinib to macrophages while minimizing system toxicity, we chose to develop and utilize a nano-formulation of this drug, as well as administer it via intraperitoneal injections. Because most ovarian cancers present and recur in the peritoneal cavity, application of intraperitoneal therapy towards this setting is possibly beneficial. A phase III trial (GOG 104) with results published in 1996 demonstrated that i.v. cyclophosphamide with i.p cisplatin significantly improved survival and had significantly fewer side effects than i.v. administration of both drugs in stage III ovarian cancer patients with residual tumor masses ≤ 2 cm. [108] However, paclitaxel soon replaced cyclophosphamide as the therapy of choice to combine with cisplatin, and the benefits seen in the GOG 104 trial were not greater than those of the new chemotherapeutic agent. Soon after, two other trials (GOG 114 and GOG 172) also demonstrated survival advantage, albeit with possible confounding factors. [109,110] More recently, another trial with over 1,500 participants (GOG 252) comparing the anti-VEGF antibody bevacizumab in combination with i.v. versus i.p. chemotherapy in ovarian, fallopian tube, and peritoneal cancers appeared to show that i.p. dosing does not confer any advantage. [111] However, survival data is not yet mature and it is unclear whether any possible difference between administration routes could have been overshadowed by ovarian cancer's inherent sensitivity to bevacizumab. In sum, the role of i.p. administration in ovarian cancer is not without controversy.

Regardless, our approach can likely also be adapted for i.v. nanoparticle administration, a treatment modality for which there already exists precedence. For example, PEGylated liposomal doxorubicin (Doxil) was approved in 1999 as a single agent for treatment of advanced ovarian cancer patients who had failed first-line platinum-based chemotherapy. [112] Additionally, i.v. administration of abraxane, an albumin-stabilized nanoparticle formulation of paclitaxel, has more recently been shown to be safe and effective in patients with recurrent ovarian cancer (NCT00499252). Because ovarian cancer subtypes enriched in MAPK dysregulation are also the ones most likely to be chemoresistant to drugs such as Doxil and abraxane, nano-formulations of RTKi represent a possible avenue for further exploration in this disease setting.

4.4 Materials and methods

In vitro cell culture assays. PrestoBlue (Invitrogen) was used as an indicator of cell viability. Conditioned media experiments were performed as described in Section 3.4, except at a single concentration of 100 nM trametinib. In some cases, either a recombinant human AXL Fc chimera protein (R&D Systems) or human HGF antibody (AB-294-NA, R&D Systems) was added to the culture. For the in vitro synergy screen, we used the following drugs up to maximum concentrations of: 333 nM trametinib, 5 μM vemurafenib, 5 μM PD0325901, 5 μM selumetinib, 3 μM foretinib, 6 μM cabozantinib, 3 μM crizotinib, 3 μM tivantinib, 6 μM R428. All inhibitors were purchased from Selleck Chem. Additionally, where indicated, recombinant GAS6, HGF, or EGF protein (PeproTech) was added. For RTK signaling measurements in mono-cultures of ES2 cells and U937-derived macrophages, a concentration of 1 μM foretinib was used.

Synergy calculation using the Loewe additivity model. Raw cell survival data following treatment with varying concentrations of drug combinations were fit to a model of Loewe additivity. [113] Matlab (Mathworks) was used to computationally infer the interaction parameter α for drug 1 combined with drug 2 via nonlinear regression:

$$1 = \frac{D_1}{IC_{50,1}\left(\frac{E}{E_{control}-E}\right)^{\frac{1}{m_1}}} + \frac{D_2}{IC_{50,2}\left(\frac{E}{E_{control}-E}\right)^{\frac{1}{m_2}}} + \frac{\propto D_1 D_2}{IC_{50,1} IC_{50,2}\left(\frac{E}{E_{control}-E}\right)^{\left(\frac{1}{2m_1}+\frac{1}{2m_1}\right)}}$$

where E = measured fractional survival

$E_{control}$ = control fractional survival = 1

D = drug concentration

IC_{50} = half maximal inhibitory concentration

m = cytotoxicity curve Hill slope

Standard error was quantified via jackknife leave-one-out cross validation.

GSEA. GSEA (Broad Institute) using a custom MAPK/ERK pathway gene set was performed on a published magnetic CRISPR screen originally aimed at identifying regulators of phagocytosis (of negatively charged 300 nm-diameter particles) in U937 cells. [105,114] The custom gene set consisted of the canonical pathway members KRAS, NRAS, HRAS, ARAF, BRAF, RAF1, MAP2K1, MAP2K2, MAPK1, MAPK3. MAP3K8 was also included, as it is a (albeit less well-known) MAPK pathway agonist that activates ERK primarily through MEK-dependent mechanisms without a requirement for RAF signaling. [115,116]

Nano-formulation and characterization. To generate nano-foretinib, 5 mg mPEG(5 kDa)-b-PCL(5 kDa) block copolymer (Advanced Polymer Materials Inc.), 1 mg 50:50 PLGA (30-60 kDa, Sigma), and 1 mg foretinib were dissolved in 300 µl DMF (Sigma). An equal volume of acetonitrile (Sigma) was added, and a nanoprecipitation procedure was performed. Briefly, while stirring, this mixed

solution was added dropwise to a volume of diH_2O 30 times that of the organic phase. After overnight stirring, the nanoparticle solution was filtered through 0.45 μm syringe filters (Whatman), then concentrated using Amicon spin filters (100 kDa, EMD Millipore). For characterization, size and zeta-potential measurements were performed via DLS (Malvern Zetasizer). For quantification of drug loaded into nanoparticles, nanoparticles were dissolved with the addition of 4 parts DMF, then run on an LC-MS with in-line photodiode array detector (Waters). Foretinib concentration within nanoparticle samples was quantified via integration of absorbance peaks at 332 nm relative to a standard curve of known foretinib concentrations.

Formulation of fluorescently labeled nanoparticles. Fluorescently labeled, foretinib-loaded nanoparticles (BODIPY630-nano-foretinib) were generated in the same fashion as their unlabeled counterparts, except PLGA labeled with BODIPY 630/650 was used in place of unlabeled PLGA. PLGA was labeled as in [117], by reacting the fluorophore amine group with the PLGA terminal carboxylic acid group. 4 mg BODIPY 630/650-NH2 (Lumiprobe) and 10 μL DIPEA was added while stirring a mixture of 200 mg 50:50 PLGA (30-60 kDa, Sigma), 16 mg EDC, and 4 mg NHS in DMF. Following overnight stirring in the dark, the labeled polymer was precipitated in cold 1:1 methanol:diethyl ether, centrifuged at 2000 g for 10 min, then re-dissolved in dichloromethane. This process was repeated 5x until the methanol:diethyl ether supernatant no longer contained free fluorophore, as verified by LC-MS with fluorescence detection. The resulting precipitate was dried under vacuum for weight quantification, then dissolved in DMF for further use.

Nanoparticle uptake studies and blood half-life measurements. Whole-body biodistribution and tumor uptake studies were performed 24 hr after i.p. injection of 30 mg/kg BODIPY630-nano-foretinib. Mice were euthanized, and relevant

organs were harvested for fluorescence reflectance imaging using an OV110 imaging system (Olympus). Fluorescence intensities were quantified following background subtraction of a PBS-treated control. Blood half-life was determined by confocal imaging of a healthy nu/nu mouse ear after i.p. injection of BODIPY630-nanoforetinib. The accumulation half-life was quantified by fitting background-subtracted fluorescence values to a one-phase association curve, while the decay half-life was quantified by fitting to a one-phase decay curve in Prism 7.0 (GraphPad).

Whole-body fluorescence imaging. For in vivo efficacy studies, i.p. tumor burden was longitudinally tracked via whole-body fluorescence imaging using the Ami HT imaging system (Spectral Instruments Imaging). Aura software (Spectral Instruments Imaging) was used to quantify total emission (photons/sec) associated with the ES2 ERK KTR (γ_{ex} = 465 nm, γ_{em} = 510 nm) within equally sized ROIs drawn around each mouse.

5 Conclusions and future directions

While targeted therapies against cancer represent an attractive therapeutic modality, they are not without disadvantages. Results from clinical trials are equivocal, with patients often exhibiting only partial responses, if any. In patients that do respond well initially, acquired resistance almost invariably develops. Many studies thus far have either focused on examining cancer cell-intrinsic resistance or interactions between specific cell types within the tumor microenvironment in a very targeted, hypothesis-driven fashion. Fewer studies have taken a more discovery-based approach, such as by computationally examining all possible interactions prior to functional validation in experimental systems.

In order to generate testable hypothesis pertaining to stromal and/or immune cell influence on tumor-intrinsic compensatory signaling, we re-analyzed previously published patient gene expression data sets to uncover possible cellular and molecular mediators of clinical MAPKi response. This led us to hypothesize that paracrine TAM-tumor interactions, as well as autocrine signaling by TAMs or tumor cells alone, might contribute to therapeutic resistance. While our analysis pointed towards the influence of growth factor-RTK signaling, ligand-receptor interactions associated with chemokines, integrins, etc. can also be considered given the specific reference list that we used, and these reference lists will only continue to grow as additional interactions are discovered and validated across various cellular contexts. Additionally, our exploratory analysis of ligand-receptor interactions focused on upstream portions of signal transduction pathways, without

any insight into their downstream activation status. Given the redundancy of RTK-triggered pathways, computational approaches for inferring downstream pathway activation may be helpful for further refining testable hypotheses. One example, developed by the Saez-Rodriguez group, uses a common core of Pathway RespOnsive GENes (PROGENy) to infer pathway activity from gene expression data. [118] This was accomplished by taking into account a large compendium of published perturbation experiments. Ultimately, additional information garnered from computational means might equate to less experimental throughput and resources being required for downstream validation.

Our lab has previously employed a "cue-signal-response" paradigm to quantitatively dissect signaling networks associated with TNF-α-induced apoptosis in colorectal cancer, T cell receptor—peptide/MHC binding in T cell functional responses, and protease activity in endometriosis, among others. [119–121] While "signals" measured at baseline can sometimes be predictive of cellular response, this is not always the case. This framework thus takes into account the importance of measuring said "signals" and phenotypic "responses" upon changes to environmental "cues". Here, we expanded upon this framework by employing computational methods to inform the designation of our experimental perturbations. To test our computationally generated hypotheses, we defined our "cues" to be MEKi administration with or without macrophage co-culture; our "signals" to be levels of total (and active, where relevant) proteins along various growth factor-RTK-intracellular kinase signaling axes; and our "responses" to be cellular growth.

In vivo, we found that macrophage infiltration increases as a result of MEKi. Because this phenomenon has also been observed in response to other forms of therapeutic insult, including radio- and chemotherapy, it may be of interest to assess whether this is simply a general anti-inflammatory response following all forms of tumor cell death. [104,122] If macrophage influx is a true prognostic

indicator, then non-invasive imaging via macrin may be worth pursuing in a clinical setting, especially in cases where tumor or metastatic sites are logistically impossible to biopsy for immunohistochemical staining.

In the specific model tested here, while macrophage depletion did not have causal effects on trametinib efficacy, we found that we could leverage trametinib-induced macrophage infiltration in the design of a combination therapy targeting tumor-macrophage growth factor-RTK crosstalk. Our results further suggest that this combination therapy not only affects intercellular signaling, but also directly modulates macrophage function. This is of particular interest because, as opposed to M1-polarized "classically activated" macrophages, which promote T helper response and exhibit tumoricidal activity, M2-polarized "alternatively activated" macrophages are known to interact with cancer cells to promote tumor development. [123] In ovarian cancer, increasing densities of CD163+ M2-polarized TAMs have been linked to higher stages of disease, and higher M2 to M1 ratios have been linked to worse prognosis. [124,125] Accordingly, attempts to shift the macrophage milieu towards a more M1-polarized phenotype have been the focus of recent immune-oncology studies, particularly for cancers regarded as immunologically cold. These tumors are still regarded as difficult-to-treat, as they often do not yield durable responses to targeted therapies, nor do they initially respond to immune checkpoint blockade. Pancreatic cancer is notorious for this due to the presence of a dense fibrotic structure that excludes immune cell infiltrates, and even certain subtypes of melanoma demonstrate primary resistance to checkpoint blockade. [126,127]

The dramatic and durable responses to immune checkpoint blockade in a subset of tumors has led to its combination with countless inhibitors, in order to capture its effects across broader patient populations. In some cases, the excessive amount of clinical trials even translates into a lack of patients available for enrolling in them. As such, the methodologies presented here may be useful for mechanistically understanding pathways leading to synergistic and/or antagonistic

effects and therefore enable more informed pre-clinical evaluations to rationally determine whether some of these combinations are even worth testing in the clinic.

In this thesis, we focused on intercellular crosstalk between two cell types, but in actuality, in vivo interactions likely feature signaling cascades involving multiple cell populations, and can be probed with high-dimensional approaches that have become increasingly accessible in recent years. Proteomic and genomic profiling tools such as mass spectrometry, mass cytometry, and scRNA-seq of dissociated tumor samples enable highly detailed snapshots of cancers subjected to various perturbations. Increasingly availability of profiles from matched patient samples will provide us with data sets most relevant to the biological questions at hand, hopefully circumventing the need to pool data from cancers or subtypes of cancers that are known to signal differently from one another. Enhanced computational methods will enable educated determination of hypotheses to pursue in a more targeted fashion. To accomplish this, multiplex bead-based immunoassays and flow cytometry can be employed to profile cell functional states, while cyclic immunofluorescence of frozen or formalin-fixed, paraffin-embedded (FFPE) tissue can provide us with high-dimensional imaging data sets. [128] Multivariate analysis of extracted image parameters, for example with histoCAT analysis, can then be used to determine whether there might be spatial requirements governing intercellular interactions of interest, and intravital imaging strategies can be applied towards visualizing and understanding signaling networks in their appropriate microenvironmental contexts. [129]

Overall, this work adds to the increasing body of knowledge showing that multiple bypass pathways operate in parallel, both as a result of and in order to effect changes in tumors and their surrounding microenvironment. Our hope is that the results from this thesis, along with its overarching computational and experimental framework, may help inform the development of not only cancer therapeutics, but also biomarker strategies for enhanced patient stratification into treatment arms.

Bibliography

[1] Lemmon MA, Schlessinger J. Cell Signaling by Receptor Tyrosine Kinases. Cell. 2010 Jun 25;141(7):1117–34.

[2] Ullrich A, Schlessinger J. Signal transduction by receptors with tyrosine kinase activity. Cell. 1990 Apr 20;61(2):203–12.

[3] Östman A, Böhmer F-D. Regulation of receptor tyrosine kinase signaling by protein tyrosine phosphatases. Trends Cell Biol. 2001 Jun 1;11(6):258–66.

[4] Haj FG, Markova B, Klaman LD, Bohmer FD, Neel BG. Regulation of receptor tyrosine kinase signaling by protein tyrosine phosphatase-1B. J Biol Chem. 2003 Jan 10;278(2):739–44.

[5] Goh LK, Sorkin A. Endocytosis of receptor tyrosine kinases. Cold Spring Harb Perspect Biol. 2013 May 1;5(5):a017459.

[6] Du Z, Lovly CM. Mechanisms of receptor tyrosine kinase activation in cancer. Mol Cancer. 2018 Dec 19;17(1):58.

[7] Sharma S V., Bell DW, Settleman J, Haber DA. Epidermal growth factor receptor mutations in lung cancer. Nat Rev Cancer. 2007 Mar 1;7(3):169–81.

[8] Slamon DJ, Godolphin W, Jones LA, Holt JA, Wong SG, Keith DE, et al. Studies of the HER-2/neu proto-oncogene in human breast and ovarian cancer. Science. 1989 May 12;244(4905):707–12.

[9] Liu C, Tsao MS. In vitro and in vivo expressions of transforming growth factor-alpha and tyrosine kinase receptors in human non-small-cell lung

carcinomas. Am J Pathol. 1993 Apr;142(4):1155–62.

[10] Olivero M, Rizzo M, Madeddu R, Casadio C, Pennacchietti S, Nicotra MR, et al. Overexpression and activation of hepatocyte growth factor/scatter factor in human non-small-cell lung carcinomas. Br J Cancer. 1996 Dec;74(12):1862–8.

[11] Hutterer M, Knyazev P, Abate A, Reschke M, Maier H, Stefanova N, et al. Axl and Growth Arrest Specific Gene 6 Are Frequently Overexpressed in Human Gliomas and Predict Poor Prognosis in Patients with Glioblastoma Multiforme. Clin Cancer Res. 2008 Jan 1;14(1):130–8.

[12] Nowell PC. Discovery of the Philadelphia chromosome: a personal perspective. J Clin Invest. 2007 Aug 1;117(8):2033–5.

[13] Sporn MB, Todaro GJ. Autocrine Secretion and Malignant Transformation of Cells. N Engl J Med. 1980 Oct 9;303(15):878–80.

[14] Tokumaru S, Higashiyama S, Endo T, Nakagawa T, Miyagawa JI, Yamamori K, et al. Ectodomain shedding of epidermal growth factor receptor ligands is required for keratinocyte migration in cutaneous wound healing. J Cell Biol. 2000 Oct 16;151(2):209–20.

[15] Walsh JH, Karnes WE, Cuttitta F, Walker A. Autocrine growth factors and solid tumor malignancy. West J Med. 1991 Aug;155(2):152–63.

[16] Krystal GW, Hines SJ, Organ CP. Autocrine growth of small cell lung cancer mediated by coexpression of c-kit and stem cell factor. Cancer Res. 1996 Jan 15;56(2):370–6.

[17] Witsch E, Sela M, Yarden Y. Roles for growth factors in cancer progression. Physiology (Bethesda). 2010 Apr;25(2):85–101.

[18] Qi J, McTigue MA, Rogers A, Lifshits E, Christensen JG, Janne PA, et al. Multiple Mutations and Bypass Mechanisms Can Contribute to Development of Acquired Resistance to MET Inhibitors. Cancer Res. 2011 Feb

1;71(3):1081–91.

[19] Sasaki T, Koivunen J, Ogino A, Yanagita M, Nikiforow S, Zheng W, et al. A Novel ALK Secondary Mutation and EGFR Signaling Cause Resistance to ALK Kinase Inhibitors. Cancer Res. 2011 Sep 15;71(18):6051–60.

[20] Zhang Z, Lee JC, Lin L, Olivas V, Au V, LaFramboise T, et al. Activation of the AXL Kinase Causes Resistance to EGFR-Targeted Therapy in Lung Cancer. Nat Genet. 2012;44(8):852.

[21] Martin GS. Cell signaling and cancer. Cancer Cell. 2003 Sep 1;4(3):167–74.

[22] Jung KH, Park BH, Hong S-S. Progress in cancer therapy targeting c-Met signaling pathway. Arch Pharm Res. 2012 Apr 3;35(4):595–604.

[23] Fruman DA, Rommel C. PI3K and cancer: lessons, challenges and opportunities. Nat Rev Drug Discov. 2014 Feb;13(2):140–56.

[24] Tournier C. The 2 Faces of JNK Signaling in Cancer. Genes Cancer. 2013 Sep;4(9–10):397.

[25] Holash J, Davis S, Papadopoulos N, Croll SD, Ho L, Russell M, et al. VEGF-Trap: A VEGF blocker with potent antitumor effects. Proc Natl Acad Sci. 2002 Aug 20;99(17):11393–8.

[26] Michieli P, Mazzone M, Basilico C, Cavassa S, Sottile A, Naldini L, et al. Targeting the tumor and its microenvironment by a dual-function decoy Met receptor. Cancer Cell. 2004 Jul 1;6(1):61–73.

[27] Kariolis MS, Miao YR, Jones DS, Kapur S, Mathews II, Giaccia AJ, et al. An engineered Axl "decoy receptor" effectively silences the Gas6-Axl signaling axis. Nat Chem Biol. 2014;10(11):977–83.

[28] Imai K, Takaoka A. Comparing antibody and small-molecule therapies for cancer. Nat Rev Cancer. 2006 Sep 1;6(9):714–27.

[29] Dhillon AS, Hagan S, Rath O, Kolch W. MAP kinase signalling pathways in

cancer. Oncogene. 2007 May 14;26(22):3279–90.

[30] Turski ML, Vidwans SJ, Janku F, Garrido-Laguna I, Munoz J, Schwab R, et al. Genomically Driven Tumors and Actionability across Histologies: BRAF-Mutant Cancers as a Paradigm. 2016;

[31] Bamford S, Dawson E, Forbes S, Clements J, Pettett R, Dogan A, et al. The COSMIC (Catalogue of Somatic Mutations in Cancer) database and website.

[32] Cantwell-Dorris ER, O'leary JJ, Sheils OM. BRAF V600E : Implications for Carcinogenesis and Molecular Therapy. Mol Cancer Ther. 2011;10(3).

[33] Davies H, Bignell GR, Cox C, Stephens P, Edkins S, Clegg S, et al. Mutations of the BRAF gene in human cancer. Nature. 2002 Jun 9;417(6892):949–54.

[34] Prior IA, Lewis PD, Mattos C. A Comprehensive Survey of Ras Mutations in Cancer. 2012;

[35] Long G V, Flaherty KT, Stroyakovskiy D, Gogas H, Levchenko E, De Braud F, et al. Dabrafenib plus trametinib versus dabrafenib monotherapy in patients with metastatic BRAF V600E/ K-mutant melanoma: long-term survival and safety analysis of a phase 3 study. Ann Oncol. 2017;28:1631–9.

[36] Planchard D, Smit EF, Groen HJM, Mazieres J, Besse B, Helland Å, et al. Dabrafenib plus trametinib in patients with previously untreated BRAFV600E-mutant metastatic non-small-cell lung cancer: an open-label, phase 2 trial. Lancet Oncol. 2017 Oct 1;18(10):1307–16.

[37] Therapeutics T, Biology C. RG7204 (PLX4032), a Selective BRAF V600E Inhibitor, Displays Potent Antitumor Activity in Preclinical Melanoma Models. 2010;

[38] Joseph EW, Pratilas CA, Poulikakos PI, Tadi M, Wang W, Taylor BS, et al. The RAF inhibitor PLX4032 inhibits ERK signaling and tumor cell proliferation in a V600E BRAF-selective manner.

[39] Lee JT, Li L, Brafford PA, van den Eijnden M, Halloran MB, Sproesser K, et al. PLX4032, a potent inhibitor of the B-Raf V600E oncogene, selectively

inhibits V600E-positive melanomas. Pigment Cell Melanoma Res. 2010 Dec 1;23(6):820–7.

[40] Rheault TR, Stellwagen JC, Adjabeng GM, Hornberger KR, Petrov KG, Waterson AG, et al. Discovery of Dabrafenib: A Selective Inhibitor of Raf Kinases with Antitumor Activity against B-Raf-Driven Tumors. ACS Med Chem Lett. 2013 Mar 14;4(3):358–62.

[41] Halaban R, Zhang W, Bacchiocchi A, Cheng E, Parisi F, Ariyan S, et al. PLX4032, a selective BRAFV600E kinase inhibitor, activates the ERK pathway and enhances cell migration and proliferation of BRAFWT melanoma cells. Pigment Cell Melanoma Res. 2010 Apr 1;23(2):190–200.

[42] Holderfield M, Merritt H, Chan J, Wallroth M, Tandeske L, Zhai H, et al. RAF Inhibitors Activate the MAPK Pathway by Relieving Inhibitory Autophosphorylation. Cancer Cell. 2013 May 13;23(5):594–602.

[43] Ryan MB, Corcoran RB. Therapeutic strategies to target RAS-mutant cancers. Nat Rev Clin Oncol. 2018 Nov 1;15(11):709–20.

[44] Janes MR, Zhang J, Li L-S, Patricelli MP, Ren P, Liu Correspondence Y. Targeting KRAS Mutant Cancers with a Covalent G12C-Specific Inhibitor In Brief A covalent inhibitor specific for G12C mutant KRAS induces tumor regression in in vivo models. Cell. 2018;172:578-581.e17.

[45] Patricelli MP, Janes MR, Li L-S, Hansen R, Peters U, Kessler L V, et al. Selective Inhibition of Oncogenic KRAS Output with Small Molecules Targeting the Inactive State. 2016;

[46] Commisso C, Davidson SM, Soydaner-Azeloglu RG, Parker SJ, Kamphorst JJ, Hackett S, et al. Macropinocytosis of protein is an amino acid supply route in Ras-transformed cells HHS Public Access. Nature. 2013;497(7451):633–7.

[47] Yang S, Wang X, Contino G, Liesa M, Sahin E, Ying H, et al. Pancreatic cancers require autophagy for tumor growth.

[48] Wang T, Yu H, Hughes NW, Liu B, Kendirli A, Klein K, et al. Gene Essentiality Profiling Reveals Gene Networks and Synthetic Lethal Interactions with Oncogenic Ras HHS Public Access. Cell. 2017;168(5):890–903.

[49] Blake JF, Burkard M, Chan J, Chen H, Chou K-J, Diaz D, et al. methyl-1H-pyrazol-5-yl)amino)pyrimidin-4-yl)pyridin-2(1H)-one (GDC-0994), an Extracellular Signal-Regulated Kinase 1/2 (ERK1/2) Inhibitor in Early Clinical Development. Discov. 2016;(1).

[50] Moschos SJ, Sullivan RJ, Hwu W-J, Ramanathan RK, Adjei AA, Fong PC, et al. Development of MK-8353, an orally administered ERK1/2 inhibitor, in patients with advanced solid tumors. JCI Insight. 2018 Feb 22;3(4).

[51] Sullivan RJ, Infante JR, Janku F, Jean Lee Wong D, Sosman JA, Keedy V, et al. First-in-Class ERK1/2 Inhibitor Ulixertinib (BVD-523) in Patients with MAPK Mutant Advanced Solid Tumors: Results of a Phase I Dose-Escalation and Expansion Study. 2017;

[52] Hatzivassiliou G, Haling JR, Chen H, Song K, Price S, Heald R, et al. Mechanism of MEK inhibition determines efficacy in mutant KRAS- versus BRAF-driven cancers. Nature. 2013 Sep 11;501(7466):232–6.

[53] Blumenschein GR, Smit EF, Planchard D, Kim D-W, Cadranel J, De Pas T, et al. A randomized phase II study of the MEK1/MEK2 inhibitor trametinib (GSK1120212) compared with docetaxel in KRAS-mutant advanced non-small-cell lung cancer (NSCLC)†. Ann Oncol Off J Eur Soc Med Oncol. 2015 May;26(5):894–901.

[54] Farley J, Brady WE, Vathipadiekal V, Lankes HA, Coleman R, Morgan MA, et al. A Phase Ii Trial Of Selumetinib (Azd6244) In Women With Recurrent Low-Grade Serous Carcinoma Of The Ovary Or Peritoneum: A Gynecologic Oncology Group Trial. Lancet Oncol. 2013;14(2):134–40.

[55] Claas AM, Atta L, Gordonov S, Meyer AS, Lauffenburger DA. Systems

Modeling Identifies Divergent Receptor Tyrosine Kinase Reprogramming to MAPK Pathway Inhibition. Cell Mol Bioeng. 2018 Dec 26;11(6):451–69.

[56] Wagle N, Van Allen EM, Treacy DJ, Frederick DT, Cooper ZA, Taylor-Weiner A, et al. MAP kinase pathway alterations in BRAF-mutant melanoma patients with acquired resistance to combined RAF/MEK inhibition. Cancer Discov. 2014;4(1):61–8.

[57] Ahronian LG, Sennott EM, Van Allen EM, Wagle N, Kwak EL, Faris JE, et al. Clinical Acquired Resistance to RAF Inhibitor Combinations in BRAF-Mutant Colorectal Cancer through MAPK Pathway Alterations. 2015;

[58] Lidsky M, Antoun G, Speicher P, Adams B, Turley R, Augustine C, et al. Mitogen-activated Protein Kinase (MAPK) Hyperactivation and Enhanced NRAS Expression Drive Acquired Vemurafenib Resistance in V600E BRAF Melanoma Cells *. 2014;

[59] Corcoran RB, Dias-Santagata D, Bergethon K, Iafrate AJ, Settleman J, Engelman JA, et al. BRAF Gene Amplification Can Promote Acquired Resistance to MEK Inhibitors in Cancer Cells Harboring the BRAF V600E Mutation. 2012;

[60] Merchant M, Moffat J, Schaefer G, Chan J, Wang X, Orr C, et al. Combined MEK and ERK inhibition overcomes therapy-mediated pathway reactivation in RAS mutant tumors. 2017;

[61] Lito P, Saborowski A, Yue J, Solomon M, Joseph E, Gadal S, et al. Disruption of CRAF-Mediated MEK Activation Is Required for Effective MEK Inhibition in KRAS Mutant Tumors. Cancer Cell. 2014 May 12;25(5):697–710.

[62] Hanafusa H, Torii S, Yasunaga T, Nishida E. Sprouty1 and Sprouty2 provide a control mechanism for the Ras/MAPK signalling pathway. Nat Cell Biol. 2002 Nov 28;4(11):850–8.

[63] Kondoh K, Nishida E. Regulation of MAP kinases by MAP kinase

phosphatases. Biochim Biophys Acta - Mol Cell Res. 2007 Aug 1;1773(8):1227–37.

[64] Duncan JS, Whittle MC, Nakamura K, Abell AN, Midland AA, Zawistowski JS, et al. Dynamic Reprogramming of the Kinome In Response to Targeted MEK Inhibition In Triple Negative Breast Cancer. Cell. 2012;149(2):307–21.

[65] Miller MA, Oudin MJ, Sullivan RJ, Wang SJ, Meyer AS, Im H, et al. Reduced Proteolytic Shedding of Receptor Tyrosine Kinases Is a Post-Translational Mechanism of Kinase Inhibitor Resistance. 2016;

[66] Wilson TR, Fridlyand J, Yan Y, Penuel E, Burton L, Chan E, et al. Widespread potential for growth-factor-driven resistance to anticancer kinase inhibitors. Nature. 2012 Jul 4;487(7408):505–9.

[67] Straussman R, Morikawa T, Shee K, Barzily-Rokni M, Qian ZR, Du J, et al. Tumour micro-environment elicits innate resistance to RAF inhibitors through HGF secretion. Nature. 2012 Jul 4;487(7408):500–4.

[68] Cheng H, Terai M, Kageyama K, Ozaki S, McCue PA, Sato T, et al. Paracrine Effect of NRG1 and HGF Drives Resistance to MEK Inhibitors in Metastatic Uveal Melanoma. Cancer Res. 2015 Jul 1;75(13):2737–48.

[69] Vella LJ, Pasam A, Dimopoulos N, Andrews M, Knights A, Puaux A-L, et al. MEK Inhibition, Alone or in Combination with BRAF Inhibition, Affects Multiple Functions of Isolated Normal Human Lymphocytes and Dendritic Cells. Cancer Immunol Res. 2014;2(4).

[70] Liu L, Mayes PA, Eastman S, Shi H, Yadavilli S, Zhang T, et al. The BRAF and MEK Inhibitors Dabrafenib and Trametinib: Effects on Immune Function and in Combination with Immunomodulatory Antibodies Targeting PD-1, PD-L1, and CTLA-4. 2015;

[71] Ebert PJR, Cheung J, Yang Y, McNamara E, Hong R, Moskalenko M, et al. MAP Kinase Inhibition Promotes T Cell and Anti-tumor Activity in Combination with PD-L1 Checkpoint Blockade. Immunity. 2016;44(3):609–

21.

[72] Eng C, Kim TW, Bendell J, Argilés G, Tebbutt NC, Di Bartolomeo M, et al. Atezolizumab with or without cobimetinib versus regorafenib in previously treated metastatic colorectal cancer (IMblaze370): a multicentre, open-label, phase 3, randomised, controlled trial. Lancet Oncol. 2019 Apr 16;

[73] Newman AM, Liu CL, Green MR, Gentles AJ, Feng W, Xu Y, et al. Robust enumeration of cell subsets from tissue expression profiles. Nat Methods. 2015 May 30;12(5):453–7.

[74] Long G V., Fung C, Menzies AM, Pupo GM, Carlino MS, Hyman J, et al. Increased MAPK reactivation in early resistance to dabrafenib/trametinib combination therapy of BRAF-mutant metastatic melanoma. Nat Commun. 2014 Dec 2;5(1):5694.

[75] Kumar MP, Du J, Lagoudas G, Jiao Y, Sawyer A, Drummond DC, et al. Analysis of Single-Cell RNA-Seq Identifies Cell-Cell Communication Associated with Tumor Characteristics. Cell Rep. 2018 Nov 6;25(6):1458-1468.e4.

[76] Tirosh I, Izar B, Prakadan SM, Wadsworth MH, Treacy D, Trombetta JJ, et al. Dissecting the multicellular ecosystem of metastatic melanoma by single-cell RNA-seq. Science. 2016 Apr 8;352(6282):189–96.

[77] Weinreb C, Wolock S, Klein AM. SPRING: a kinetic interface for visualizing high dimensional single-cell expression data. Berger B, editor. Bioinformatics. 2018 Apr 1;34(7):1246–8.

[78] Ramilowski JA, Goldberg T, Harshbarger J, Kloppmann E, Lizio M, Satagopam VP, et al. A draft network of ligand–receptor-mediated multicellular signalling in human. Nat Commun. 2015 Dec 22;6(1):7866.

[79] Southan C, Sharman JL, Benson HE, Faccenda E, Pawson AJ, Alexander SPH, et al. The IUPHAR/BPS Guide to PHARMACOLOGY in 2016: towards curated quantitative interactions between 1300 protein targets and

6000 ligands. Nucleic Acids Res. 2016 Jan 4;44(D1):D1054–68.

[80] Laoui D, Van Overmeire E, Conza G Di, Aldeni C, Keirsse J, Morias Y, et al. Tumor Hypoxia Does Not Drive Differentiation of Tumor-Associated Macrophages but Rather Fine-Tunes the M2-like Macrophage Population. 2014;

[81] Dijkgraaf EM, Heusinkveld M, Tummers B, Vogelpoel LTC, Goedemans R, Jha V, et al. Chemotherapy Alters Monocyte Differentiation to Favor Generation of Cancer-Supporting M2 Macrophages in the Tumor Microenvironment. Cancer Res. 2013 Apr 15;73(8):2480–92.

[82] Kasikara C, Kumar S, Kimani S, Tsou W-I, Geng K, Davra V, et al. Phosphatidylserine Sensing by TAM Receptors Regulates AKT-Dependent Chemoresistance and PD-L1 Expression. Mol Cancer Res. 2017;15(6):753–64.

[83] Anglesio MS, Arnold JM, George J, Tinker A V., Tothill R, Waddell N, et al. Mutation of ERBB2 Provides a Novel Alternative Mechanism for the Ubiquitous Activation of RAS-MAPK in Ovarian Serous Low Malignant Potential Tumors. Mol Cancer Res. 2008 Nov 1;6(11):1678–90.

[84] Matsuo K, Machida H, Grubbs BH, Sood AK, Gershenson DM. Trends of low-grade serous ovarian carcinoma in the United States. J Gynecol Oncol. 2018;29(1):e15.

[85] Segura E, Touzot M, Bohineust A, Cappuccio A, Chiocchia G, Hosmalin A, et al. Human inflammatory dendritic cells induce Th17 cell differentiation. Immunity. 2013 Feb 21;38(2):336–48.

[86] Gao Q, Yang Z, Xu S, Li X, Yang X, Jin P, et al. Heterotypic CAF-tumor spheroids promote early peritoneal metastatis of ovarian cancer. J Exp Med. 2019 Mar 4;216(3):688–703.

[87] Stanford JC, Young C, Hicks D, Owens P, Williams A, Vaught DB, et al. Efferocytosis produces a prometastatic landscape during postpartum

mammary gland involution. J Clin Invest. 2014;124(11):4737–52.

[88] Seitz HM, Camenisch TD, Lemke G, Earp HS, Matsushima GK. Macrophages and dendritic cells use different Axl/Mertk/Tyro3 receptors in clearance of apoptotic cells. J Immunol. 2007;178(9):5635–42.

[89] Regot S, Hughey JJ, Bajar BT, Carrasco S, Covert MW. High-Sensitivity Measurements of Multiple Kinase Activities in Live Single Cells. Cell. 2014 Jun 19;157(7):1724–34.

[90] Wang T, Xiao M, Ge Y, Krepler C, Belser E, Lopez-Coral A, et al. BRAF inhibition stimulates melanoma-associated macrophages to drive tumor growth. Clin Cancer Res. 2015;21(7):1652–64.

[91] Smith MP, Sanchez-Laorden B, O'brien K, Brunton H, Ferguson J, Young H, et al. The immune microenvironment confers resistance to MAPK pathway inhibitors through macrophage-derived TNF—. Cancer Discov. 2014;4(10):1214–29.

[92] Yin M, Li X, Tan S, Zhou HJ, Ji W, Bellone S, et al. Tumor-associated macrophages drive spheroid formation during early transcoelomic metastasis of ovarian cancer. J Clin Invest. 2016 Nov 1;126(11):4157–73.

[93] Azenshtein E, Luboshits G, Shina S, Neumark E, Shahbazian D, Weil M, et al. The CC Chemokine RANTES in Breast Carcinoma Progression. Cancer Res. 2002;62(4):1093–102.

[94] Suarez-Carmona M, Valous NA, Charoentong P, Kather JN, Hampel M, Lenoir BMA, et al. Abstract A114: Omental fat in ovarian cancer induces metabolic and immune alterations. In: Tackling the Tumor Microenvironment: Beyond T-cells. American Association for Cancer Research; 2019. p. A114–A114.

[95] Halama N, Zoernig I, Berthel A, Kahlert C, Klupp F, Suarez-Carmona M, et al. Tumoral Immune Cell Exploitation in Colorectal Cancer Metastases

Can Be Targeted Effectively by Anti-CCR5 Therapy in Cancer Patients. Cancer Cell. 2016 Apr 11;29(4):587–601.

[96] Long ME, Eddy WE, Gong K-Q, Lovelace-Macon LL, McMahan RS, Charron J, et al. MEK1/2 Inhibition Promotes Macrophage Reparative Properties. J Immunol. 2016;198(2):862–72.

[97] Zeke A, Misheva M, Reményi A, Bogoyevitch MA. JNK Signaling: Regulation and Functions Based on Complex Protein-Protein Partnerships. Microbiol Mol Biol Rev. 2016 Sep 1;80(3):793–835.

[98] Fallahi-Sichani M, Moerke NJ, Niepel M, Zhang T, Gray NS, Sorger PK. Systematic analysis of BRAFV600E melanomas reveals a role for JNK/c-Jun pathway in adaptive resistance to drug-induced apoptosis. Mol Syst Biol. 2015 Mar 1;11(3):797.

[99] Kim J-H, Lee SC, Ro J, Kang HS, Kim HS, Yoon S. Jnk signaling pathway-mediated regulation of Stat3 activation is linked to the development of doxorubicin resistance in cancer cell lines. Biochem Pharmacol. 2010 Feb 1;79(3):373–80.

[100] Nguyen T V., Sleiman M, Moriarty T, Herrick WG, Peyton SR. Sorafenib resistance and JNK signaling in carcinoma during extracellular matrix stiffening. Biomaterials. 2014 Jul 1;35(22):5749–59.

[101] Stinchcombe TE, Johnson GL. MEK Inhibition in Non-Small Cell Lung Cancer. Lung Cancer. 2014 Nov;86(2):121.

[102] Jing Y, Zhang Z, Ma P, An S, Shen Y, Zhu L, et al. Concomitant BET and MAPK blockade for effective treatment of ovarian cancer. Oncotarget. 2016 Jan 19;7(3):2545–54.

[103] Walker DK, Abel S, Comby P, Muirhead GJ, Nedderman ANR, Smith DA. Species differences in the disposition of the CCR5 antagonist, UK-427,857, a new potential treatment for HIV. 2005;

[104] Kim HY, Li R, Ng TSC, Courties G, Rodell CB, Prytyskach M, et al. Quantitative Imaging of Tumor-Associated Macrophages and Their Response to Therapy Using 64 Cu-Labeled Macrin. ACS Nano. 2018;12(12):12015–29.

[105] Haney MS, Bohlen CJ, Morgens DW, Ousey JA, Barkal AA, Tsui CK, et al. Identification of phagocytosis regulators using magnetic genome-wide CRISPR screens. Nat Genet. 2018 Dec 5;50(12):1716–27.

[106] Liu P, Zhao L, Pol J, Levesque S, Petrazzuolo A, Pfirschke C, et al. Crizotinib-induced immunogenic cell death in non-small cell lung cancer. Nat Commun. 2019 Dec 2;10(1):1486.

[107] Tesniere A, Panaretakis T, Kepp O, Apetoh L, Ghiringhelli F, Zitvogel L, et al. Molecular characteristics of immunogenic cancer cell death. Cell Death Differ. 2008;15(1):3–12.

[108] Alberts DS, Liu PY, Hannigan E V., O'Toole R, Williams SD, Young JA, et al. Intraperitoneal Cisplatin plus Intravenous Cyclophosphamide versus Intravenous Cisplatin plus Intravenous Cyclophosphamide for Stage III Ovarian Cancer. N Engl J Med. 1996 Dec 26;335(26):1950–5.

[109] Markman M, Bundy BN, Alberts DS, Fowler JM, Clark-Pearson DL, Carson LF, et al. Phase III trial of standard-dose intravenous cisplatin plus paclitaxel versus moderately high-dose carboplatin followed by intravenous paclitaxel and intraperitoneal cisplatin in small-volume stage III ovarian carcinoma: an intergroup study of the Gynecologic Oncology Group, Southwestern Oncology Group, and Eastern Cooperative Oncology Group. J Clin Oncol. 2001 Feb 15;19(4):1001–7.

[110] Armstrong DK, Bundy B, Wenzel L, Huang HQ, Baergen R, Lele S, et al. Intraperitoneal Cisplatin and Paclitaxel in Ovarian Cancer. N Engl J Med. 2006 Jan 5;354(1):34–43.

[111] Walker J, Brady M, DiSilvestro P, Fujiwara K, Alberts D, Zheng W, et al.

A phase III trial of bevacizumab with IV versus IP chemotherapy for ovarian, fallopian tube, and peritoneal carcinoma: An NRG Oncology Study. 2016;

[112] Muggia FM, Hainsworth JD, Jeffers S, Miller P, Groshen S, Tan M, et al. Phase II study of liposomal doxorubicin in refractory ovarian cancer: antitumor activity and toxicity modification by liposomal encapsulation. J Clin Oncol. 1997 Mar 21;15(3):987–93.

[113] Greco WR, Bravo G, Parsons JC. The search for synergy: a critical review from a response surface perspective. Pharmacol Rev. 1995;47(2).

[114] Subramanian A, Tamayo P, Mootha VK, Mukherjee S, Ebert BL, Gillette MA, et al. Gene set enrichment analysis: A knowledge-based approach for interpreting genome-wide expression profiles. Proc Natl Acad Sci. 2005 Oct 25;102(43):15545–50.

[115] Johannessen CM, Boehm JS, Kim SY, Thomas SR, Wardwell L, Johnson LA, et al. COT drives resistance to RAF inhibition through MAP kinase pathway reactivation. Nature. 2010 Dec 24;468(7326):968–72.

[116] Gruosso T, Garnier C, Abelanet S, Kieffer Y, Lemesre V, Bellanger D, et al. MAP3K8/TPL-2/COT is a potential predictive marker for MEK inhibitor treatment in high-grade serous ovarian carcinomas. Nat Commun. 2015 Dec 12;6(1):8583.

[117] Miller MA, Gadde S, Pfirschke C, Engblom C, Sprachman MM, Kohler RH, et al. Predicting therapeutic nanomedicine efficacy using a companion magnetic resonance imaging nanoparticle. Sci Transl Med. 2015 Nov 18;7(314):314ra183.

[118] Schubert M, Klinger B, Klünemann M, Sieber A, Uhlitz F, Sauer S, et al. Perturbation-response genes reveal signaling footprints in cancer gene expression. Nat Commun. 2018 Dec 2;9(1):20.

[119] Janes KA, Kelly JR, Gaudet S, Albeck JG, Sorger PK, Lauffenburger DA. Cue-Signal-Response Analysis of TNF-Induced Apoptosis by Partial Least

Squares Regression of Dynamic Multivariate Data. J Comput Biol. 2004 Aug 20;11(4):544–61.

[120] Kemp ML, Wille L, Lewis CL, Nicholson LB, Lauffenburger DA. Quantitative network signal combinations downstream of TCR activation can predict IL-2 production response. J Immunol. 2007 Apr 15;178(8):4984–92.

[121] Miller MA, Meyer AS, Beste MT, Lasisi Z, Reddy S, Jeng KW, et al. ADAM-10 and -17 regulate endometriotic cell migration via concerted ligand and receptor shedding feedback on kinase signaling. Proc Natl Acad Sci U S A. 2013 May 28;110(22):E2074-83.

[122] Miller MA, Chandra R, Cuccarese MF, Pfirschke C, Engblom C, Stapleton S, et al. Radiation therapy primes tumors for nanotherapeutic delivery via macrophage-mediated vascular bursts. Sci Transl Med. 2017 May 31;9(392):eaal0225.

[123] Mantovani A, Sica A, Sozzani S, Allavena P, Vecchi A, Locati M. The chemokine system in diverse forms of macrophage activation and polarization. Trends Immunol. 2004 Dec;25(12):677–86.

[124] Zhang M, He Y, Sun X, Li Q, Wang W, Zhao A, et al. A high M1/M2 ratio of tumor-associated macrophages is associated with extended survival in ovarian cancer patients. J Ovarian Res. 2014 Feb 8;7(1):19.

[125] Takaishi K, Komohara Y, Tashiro H, Ohtake H, Nakagawa T, Katabuchi H, et al. Involvement of M2-polarized macrophages in the ascites from advanced epithelial ovarian carcinoma in tumor progression via Stat3 activation. Cancer Sci. 2010 Jul 28;101(10):2128–36.

[126] Laheru D, Jaffee EM. Immunotherapy for pancreatic cancer — science driving clinical progress. Nat Rev Cancer. 2005 Jun 20;5(6):459–67.

[127] Sharma P, Hu-Lieskovan S, Wargo JA, Ribas A. Primary, Adaptive, and Acquired Resistance to Cancer Immunotherapy. Cell. 2017;168(4):707–23.

[128] Lin J-R, Izar B, Wang S, Yapp C, Mei S, Shah PM, et al. Highly multiplexed immunofluorescence imaging of human tissues and tumors using t-CyCIF and conventional optical microscopes. Elife. 2018 Jul 11;7.

[129] Schapiro D, Jackson HW, Raghuraman S, Fischer JR, Zanotelli VRT, Schulz D, et al. histoCAT: analysis of cell phenotypes and interactions in multiplex image cytometry data. Nat Methods. 2017 Sep 7;14(9):873–6.